

# $\kappa$ ALDo 2.0: Scalable Thermal Transport from First Principles and Machine Learning Potentials

Giuseppe Barbalinardo<sup>\*,a</sup>, Zekun Chen<sup>\*,a</sup>, Dylan Folkner<sup>a</sup>, Bohan Li<sup>a,c</sup>, Nicholas Lundgren<sup>a</sup>, Nathaniel Troup<sup>a</sup>, Alfredo Fiorentino<sup>b,d</sup>, Davide Donadio<sup>a</sup>

*Department of Chemistry University of California Davis Davis CA 95616 USA*

*PSI Center for Scientific Computing Theory and Data 5232 Villigen PSI Switzerland*

*Massachusetts Institute of Technology Cambridge MA USA*

*National Centre for Computational Design and Discovery of Novel Materials (MARVEL) 5232 Villigen PSI Switzerland*

---

## Abstract

We introduce  $\kappa$ ALDo 2.0, an open-source Python package for computing vibrational, elastic, and thermal transport properties of crystalline and disordered solids from first principles and machine-learned interatomic potentials. Building on the anharmonic lattice dynamics (ALD) framework,  $\kappa$ ALDo 2.0 provides efficient CPU and GPU-accelerated implementations of the Boltzmann transport equation (BTE) for crystals and the quasi-harmonic Green-Kubo (QHGK) method. The QHGK formalism extends thermal transport predictions beyond translationally-invariant crystals to materials lacking long-range order, including glasses, alloys, and complex nanostructures.  $\kappa$ ALDo 2.0 introduces native integration with modern machine-learned potentials (MLPs), enabling thermal transport workflows that combine the accuracy of first-principles methods with the scalability of classical force fields. It also features comprehensive support for temperature-dependent effective potentials (TDEP) workflows, flexible storage backends for large-scale calculations, and advanced quantification of anharmonicity.

The software seamlessly interfaces with electronic structure codes (Quantum ESPRESSO, VASP), molecular dynamics packages (LAMMPS), and state-of-the-art MLPs (ACE, NEP, MACE, MatterSim, Orb), enabling thermal transport studies from 0 K to finite temperatures.  $\kappa$ ALDo 2.0 implements multiple BTE solution strategies (relaxation time approximation, self-consistent iteration, full matrix inversion) and supports essential physical corrections, including isotopic scattering and non-analytical terms for polar materials. A modular Python architecture with lazy evaluation and multiple storage formats (formatted text, NumPy, HDF5) enables simulations of systems containing up to tens of thousands of atoms.

This paper describes the theoretical framework, implementation details, software architecture, and validation examples demonstrating  $\kappa$ ALDo 2.0's capabilities for studying complex materials, including halide perovskites with strong anharmonicity and polar oxides requiring long-range electrostatic corrections.

---

*Email addresses:* gbarbalinardo@ucdavis.edu (Giuseppe Barbalinardo<sup>\*,a</sup>), ddonadio@ucdavis.edu (Davide Donadio<sup>a,d</sup>)

---

*Tags: Python, Materials Science, Computational Physics, Lattice Dynamics, Thermal Conductivity, Boltzmann Transport Equation, Machine Learning Potentials, Green-Kubo, Phonon Scattering, GPU Acceleration, TDEP, Anharmonic Effects*

**Program Title:**  $\kappa$ ALDo 2.0

**CPC Library link to program files:** (to be assigned)

**Developer's repository:** <https://github.com/nanotheorygroup/kaldo>

**Examples repository:** <https://github.com/nanotheorygroup/kaldo-examples>

**Licensing provisions:** BSD 3-Clause License

**Programming language:** Python 3.10+

**External libraries:** NumPy [1], SciPy [2], TensorFlow [3], ASE [4], sparse, opt\_einsum [5], h5py [6], seekpath [7]

**Nature of problem:** Accurate prediction of lattice heat transport in solids requires the calculation of anharmonic interatomic force constants, phonon scattering processes, and solution of the Boltzmann transport equation (BTE) for crystals or alternative formalisms for disordered materials where BTE assumptions break down. A modern software to compute lattice thermal conductivity needs: (i) flexibility to handle both crystalline and disordered materials within a unified framework, (ii) support for finite-temperature renormalization effects critical in phase-changing materials, (iii) integration with modern machine-learned potentials, or (iv) scalability to systems with thousands of atoms. A unified platform is needed that seamlessly extends the calculation of lattice thermal conductivity from crystals, including strongly anharmonic crystals, to amorphous solids while combining first-principles accuracy with computational efficiency.

**Solution method:**  $\kappa$ ALDo 2.0 implements anharmonic lattice dynamics with modular support for multiple force constant generation methods (finite differences, perturbation theory, fitting from MD trajectories) and thermal conductivity solvers: BTE (RTA, self-consistent, full matrix inversion) for crystalline materials, and quasi-harmonic Green-Kubo (QHGK) for strongly anharmonic and disordered systems. The QHGK implementation extends lattice dynamics predictions to materials lacking translational symmetry, bridging the gap between traditional BTE and molecular dynamics. The code uses sparse tensor representations and GPU acceleration via TensorFlow for the computationally intensive projection of third-order force constants onto phonon eigenstates. Multiple storage backends enable memory-efficient caching of intermediate results. Integration with ASE and various native interfaces (LAMMPS, Quantum-Espresso, etc.) provides access to diverse force calculators, including modern MLPs.

**Additional comments:**  $\kappa$ ALDo 2.0 is particularly suited for: (i) materials with strong temperature-dependent anharmonicity (e.g., halide perovskites, materials near phase transitions), (ii) studies requiring systematic comparison of multiple thermal conductivity solution methods, (iii) large-scale materials screening workflows, and (iv) development and testing of new theoretical methods in phonon transport. The software includes extensive test coverage, Docker deployment, Google Colab tutorials, and auto-generated API documentation. No special hardware is required, though GPU access significantly accelerates calculations for systems with unit cells containing over 100 atoms.

---

\*These authors contributed equally to this work

# Introduction

Thermal management has emerged as a critical challenge in modern technology, from microelectronics miniaturization to thermoelectric energy conversion and thermal barrier coatings. As device dimensions approach the nanoscale, classical continuum approaches to heat transport break down, necessitating atomistic descriptions of phonon-mediated thermal conductivity [8, 9]. Understanding and predicting thermal transport at the atomistic level is essential for materials design in applications ranging from heat dissipation in high-power electronics to efficiency optimization in energy conversion devices [10].

The past decade has witnessed remarkable progress in computational materials science driven by three converging developments. First, large-scale materials databases [11, 12, 13] have enabled systematic screening of compounds across chemical space, identifying promising candidates for targeted properties. Second, advances in high-performance computing and algorithmic improvements have extended the reach of *ab initio* methods to increasingly complex systems [14]. Third, machine learning has revolutionized interatomic potential development, initially with specialized models that achieve near-DFT accuracy at computational scaling and overall cost comparable to empirical potentials [15, 16, 17, 18, 19, 20, 21, 22], and, more recently, with foundation models that cover a large portion of the periodic table [23, 24, 25, 26].

In semiconductors and insulators, thermal transport is governed by phonons, quantized lattice vibrations arising from collective atomic motion. Molecular dynamics (MD) provides a direct route to compute thermal conductivity, either through the equilibrium Green-Kubo formalism (EMD) [27, 28, 29, 30] or via non-equilibrium approaches (NEMD) that impose a temperature gradient across the simulation cell [31, 32]. A key strength of MD is that it captures the anharmonicity of the potential energy surface to all orders, making no perturbative truncation. Moreover, MD is straightforwardly applicable to complex systems such as nanostructured, defective, and disordered materials, where the lack of translational symmetry makes reciprocal-space methods impractical. Both EMD [33, 34, 35, 36] and NEMD can be combined with empirical, machine-learned, or first-principles [37] force evaluations. However, MD-based methods face fundamental and practical limitations: (i) classical MD cannot capture quantum phonon populations, (ii) achieving size and time convergence may involve high computational cost, particularly for NEMD where finite-size extrapolation is required [32], and (iii) decomposing the total conductivity into mode-specific contributions is challenging, thus limiting physical insight.

Anharmonic lattice dynamics (ALD) offers a complementary approach that addresses these limitations [38, 39]. By computing phonon frequencies, lifetimes, and transport properties from interatomic force constants (IFCs), ALD achieves favorable scaling: computational cost grows with the number of phonon modes ( $3N$ , where  $N$  is the number of atoms) rather than MD timesteps. The Boltzmann transport equation (BTE) framework [38] enables systematic treatment of phonon-phonon scattering, isotopic disorder, and boundary effects, while providing mode-resolved analysis unavailable from EMD.

Recent theoretical advances have broadened the applicability of ALD. Unified theories, such as the Wigner approach and the quasi-harmonic Green-Kubo (QH GK) method [40, 41], have extended lattice dynamics to strongly anharmonic crystals and disordered materials, including glasses, alloys, and partially disordered nanostructures, for which interband energy transfer provides a substantial contribution to thermal transport [42, 43, 44, 45, 46][47]. Temperature-dependent effective potentials (TDEP) [48, 49, 50] enable treatment of strong anharmonicity, nuclear quantum

effects, and temperature-induced renormalization of both harmonic and anharmonic vibrational properties [51].

Whereas most of the codes available to perform ALD calculations of thermal transport (ShengBTE[52], Phono3py [53], Phoebe [54], ALAMODE [55], THERMACOND [56], and Thermal2 [57, 58]) are designed to target crystalline systems by first principles,  $\kappa$ ALDo 2.0 is created to address complex materials and acts as a native Python bridge among modern MLPs, TDEP, and advanced transport formalisms (BTE and QHGK). It unifies BTE and QHGK methods with seamless integration to modern force calculators (DFT codes, LAMMPS, MLPs) and GPU acceleration. Version 2.0 features: (i) multiple BTE solvers (RTA, self-consistent, full inversion, eigendecomposition), (ii) comprehensive physical corrections (isotopes, non-analytical terms, finite-size effects), (iii) modular storage backends enabling up to 10,000 atom systems, and (iv) extensive documentation and containerized deployment.

This paper is organized as follows. Section 2 presents the theoretical foundations and computational algorithms. Section 2.5 describes advanced physical modeling capabilities and software infrastructure. Section 3 demonstrates  $\kappa$ ALDo 2.0’s capabilities through applications to CsPbBr<sub>3</sub> halide perovskite and MgO oxide. Section 4 summarizes key features and future directions.

## Theory and Implementation

$\kappa$ ALDo 2.0 implements a hierarchical workflow for thermal transport calculations, progressing from atomic structure and interatomic force constants through phonon properties to thermal conductivity. This modular design mirrors the underlying physics while enabling flexible, efficient computation across diverse material systems. The three core components, ForceConstants, Phonons, and Conductivity classes, form the foundation of the software architecture (Fig. 2).

### Computational Workflow

Thermal transport calculations in  $\kappa$ ALDo 2.0 proceed through three main stages:

**Stage 1: Force Constant Generation or Import.** Second and third-order interatomic force constants (IFCs) are computed or imported. These tensors, encoding harmonic and anharmonic interatomic interactions, serve as the input for all subsequent analysis. Methods include: (i) finite-difference calculations with user-specified atomic displacements, (ii) direct import from density functional perturbation theory (DFPT) calculations, (iii) extraction from molecular dynamics trajectories via TDEP, or (iv) loading from external codes in various file formats (Fig. 1).

**Stage 2: Phonon Property Computation.** The dynamical matrix constructed from second-order IFCs is diagonalized to obtain phonon frequencies, eigenvectors, and group velocities. Third-order IFCs are projected onto phonon eigenstates to compute scattering phase space and rates. This computationally intensive step uses sparse tensor operations and optional GPU acceleration. Additional properties, including mode-resolved heat capacity, populations (Bose-Einstein or classical), and optional isotopic scattering rates, are calculated.

**Stage 3: Thermal Conductivity Calculation.** The BTE or QHGK formalism is employed using phonon properties from Stage 2. Multiple solution methods are available depending on accuracy requirements, memory constraints, and material characteristics. Results include mode-resolved thermal conductivity tensors, mean free paths, and optional diffusivities.

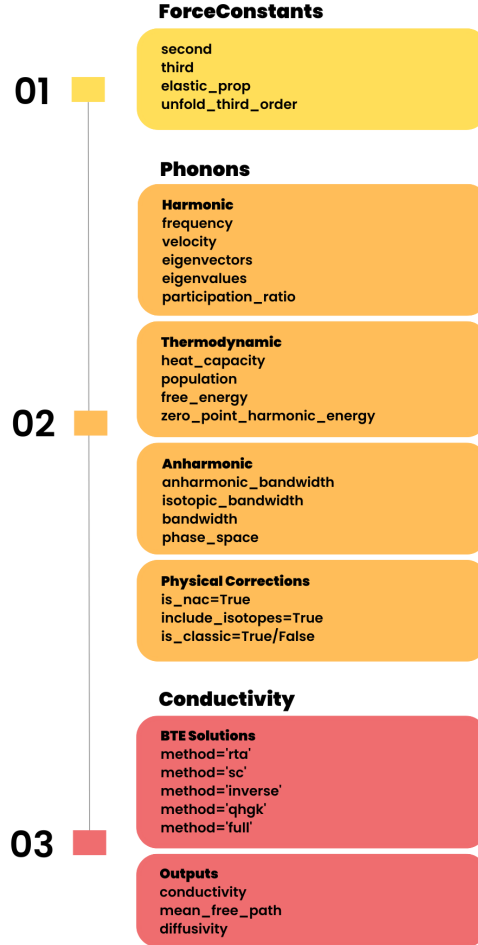


**Figure 1**  $\kappa$ ALDo 2.0 input/output ecosystem. The software interfaces with diverse force constant sources, including *ab initio* codes (Quantum ESPRESSO, VASP), molecular dynamics packages (LAMMPS), TDEP, machine-learned potentials via ASE (NEP, MACE/MatterSim, Orb), and external phonon codes (ShengBTE, phono3py, HiPhive). The workflow progresses from force constant import/generation to phonon property calculation to thermal conductivity evaluation via BTE or QHGK methods.

## Interatomic Force Constants

The first step of the ALD computation of thermal transport is the calculation of the harmonic and anharmonic force constants. In the standard lattice dynamics approach, these are the second-order,  $K^{(2)} = \{\phi''_{i\alpha i' \alpha'}\}$ , and higher-order derivatives of the potential energy surface with respect to atomic displacements. Anharmonic force constants are usually limited to third derivatives,  $K^{(3)} = \{\phi'''_{i\alpha i' \alpha' i'' \alpha''}\}$ , corresponding to three-phonon processes, although four-phonon processes are



**Figure 2**  $\kappa$ ALDo 2.0 object-oriented class structure. **ForceConstants** manages second- and third-order IFCs with methods for importing from external codes (`from_folder()`) or direct calculation via ASE (`from_ase()`). **Phonons** computes vibrational properties including frequencies, velocities, scattering rates, heat capacities, and populations. **Conductivity** solves for thermal transport via BTE (RTA, self-consistent, inverse, eigendecomposition) or QHGK methods, with outputs including thermal conductivity tensors, mean free paths, and diffusivities. All classes inherit from `Storable`, implementing lazy evaluation and flexible storage backends.

critical to capture the correct  $\kappa$  of high-conductivity materials, such as diamond, graphene, and BAs [59, 60]. In finite temperature approaches, e.g., TDEP,  $K^{(2)}$  and  $K^{(3)}$ , are numerical estimates of the derivatives of the Gibbs free energy [49, 51]. Either way,  $K^{(2)}$  and  $K^{(3)}$  are second-order and third-order tensors.

The mass-scaled second-order IFCs define the dynamical matrix elements:

$$D_{i\alpha i' \beta} = \frac{K_{i\alpha i' \beta}^{(2)}}{\sqrt{m_i m_{i'}}}, \tag{1}$$

where  $m_i$  is the mass of atom  $i$ . Phonon frequencies  $\omega_\mu$  and polarization vectors  $\eta_{i\alpha\mu}$  (mode index

$\mu$ ) satisfy the eigenvalue equation:

$$\sum_{i'\beta} D_{i\alpha i'\beta} \eta_{i'\beta\mu} = \omega_{\mu}^2 \eta_{i\alpha\mu}. \quad (2)$$

For periodic crystals, translational symmetry enables reciprocal-space formulation. The dynamical matrix at wavevector  $\mathbf{q}_k$  is:

$$D_{i\alpha k i'\beta} = \sum_{\mathbf{R}_l} e^{-i\mathbf{q}_k \cdot \mathbf{R}_l} D_{i\alpha l i'\beta}, \quad (3)$$

where  $\mathbf{R}_l$  indexes unit cell replicas. The eigenvalue problem becomes:

$$\sum_{i'\beta} D_{i\alpha k i'\beta} \eta_{i'\beta ks} = \omega_{ks}^2 \eta_{i\alpha ks}, \quad (4)$$

with band index  $s$  and wavevector index  $k$ . The composite index  $\mu = (k, s)$  labels individual phonon modes. The acoustic sum rule, ensuring zero frequency for the three acoustic modes at  $\Gamma$  ( $\mathbf{q} = 0$ ), can be enforced via the `is_acoustic_sum` flag.

## Implementation and Interfaces

The `ForceConstants` class provides a unified interface for importing and manipulating IFC files. The class method `from_folder()` supports multiple input formats listed in Table 1. Additionally, the `from_ase()` method enables direct IFCs calculations from any ASE-compatible calculator, providing access to all modern machine-learned potentials (NEP, MACE, MatterSim, Orb, etc.) as well as classical force fields and DFT codes. This flexible design enables seamless integration with diverse computational workflows.

**Table 1** Supported force constant file formats in `κALDo` 2.0, enabling integration with diverse computational workflows.

Source	Format String	Second-Order Files	Third-Order Files
Numpy	numpy	second.npy	third.npz or third.npy
LAMMPS	lammmps	Dyn.form	THIRD
VASP + ShengBTE	vasp-sheng	FORCE_CONSTANTS_2ND or FORCE_CONSTANTS	FORCE_CONSTANTS_3RD
QE + ShengBTE <sup>a</sup>	qe-sheng	espresso.ifc2	FORCE_CONSTANTS_3RD
VASP + d3q <sup>b</sup>	vasp-d3q	FORCE_CONSTANTS_2ND or FORCE_CONSTANTS	FORCE_CONSTANTS_3RD_D3Q
QE + d3q	qe-d3q	espresso.ifc2	FORCE_CONSTANTS_3RD_D3Q
HiPhive	hiphive	model2.fcs	model3.fcs
TDEP	tdep	infile.forceconstant	infile.forceconstant_thirdorder

<sup>a</sup>It supports loading force constants with mixed formats. Here, it means that the second-order force constant comes from Quantum Espresso and the third-order force comes from `thirdorder.py` in ShengBTE [52].

<sup>b</sup>The second-order force constant comes from VASP and the third-order force constant comes from Thermal2 (D3Q) [57, 58].

A key capability introduced in version 2.0 is a native support for temperature-dependent effective potentials (TDEP) [48, 50, 51]. TDEP extracts renormalized force constants from molecular dynamics trajectories, capturing anharmonic effects and temperature-induced soft mode stabilization critical in materials undergoing structural phase transitions. The typical workflow involves: (i) running

finite-temperature MD with an appropriate interatomic potential (DFT-based or MLP), (ii) processing the trajectory with TDEP tools to fit effective IFCs, and (iii) importing the resulting force constants into  $\kappa$ ALDo via the tdep format.

Integration with machine-learned potentials (MLPs) proceeds through two primary pathways: Direct ASE [4] calculators wrapping MLP implementations or LAMMPS PHONON package[61], enabling force evaluations during finite-difference IFC computation. Alternatively, MLPs can be employed within GPUMD [62] and ASE for large-scale MD simulations, with forces extracted during post-processing via TDEP. Supported MLPs include NEP [21], MACE [26], MatterSim [24], Orb [25], DeepMD [63], and others accessible through ASE or LAMMPS interfaces.

For a system with  $N_b$  atoms in the unit cell and  $N$  atoms in the supercell representation, a second-order IFC tensor has a maximum size of  $3N_b \times 3N$  elements and is always stored as a dense matrix. Third-order force constants are stored as sparse tensors (SciPy COO format) to manage memory for large systems, where the dense representation would require  $3N_b \times (3N)^2$  elements to be stored. To achieve a sparse representation while retaining good accuracy, users can specify a `third_energy_threshold` to discard negligible matrix elements, Distance-based truncation via `distance_threshold` further compresses the representation of the anharmonic IFC tensor by neglecting interactions beyond a specified cutoff radius. This approximation is valid for short-range interactions, and convergence needs to be verified for each system.

## Phonon Properties and Scattering

The Phonons class computes vibrational properties and phonon scattering rates from force constants. Core functionality includes frequency and eigenvector calculation (Eq. 4), group velocity evaluation via the Hellmann-Feynman theorem, and three-phonon scattering matrix construction.

### Group Velocities

Phonon group velocity, governing energy transport, is computed as:

$$v_{\mu\alpha} = \frac{\partial \omega_\mu}{\partial q_\alpha} = \frac{1}{2\omega_\mu} \sum_{i\beta i'\beta'} \eta_{i\beta\mu}^* \frac{\partial D_{i\beta i'\beta'}(\mathbf{q})}{\partial q_\alpha} \eta_{i'\beta'\mu}, \quad (5)$$

implemented via finite-difference evaluation of  $\partial D / \partial q_\alpha$  or analytic derivatives when available from IFC spatial Fourier transforms.

### Phonon Populations and Heat Capacity

The equilibrium phonon population follows Bose-Einstein statistics:

$$n_\mu(T) = \frac{1}{e^{\hbar\omega_\mu/k_B T} - 1}, \quad (6)$$

or in the classical limit ( $k_B T \gg \hbar\omega_\mu$ ),  $n_\mu^{\text{cl}} = k_B T / (\hbar\omega_\mu)$ . The modal heat capacity is:

$$c_\mu = k_B \left( \frac{\hbar\omega_\mu}{k_B T} \right)^2 \frac{e^{\hbar\omega_\mu/k_B T}}{(e^{\hbar\omega_\mu/k_B T} - 1)^2} = \hbar\omega_\mu \frac{\partial n_\mu}{\partial T}, \quad (7)$$

reducing to  $c_\mu^{\text{cl}} = k_B$  classically. The flag `is_classic` controls which statistics are employed.

### Three-Phonon Scattering

Anharmonic three-phonon scattering arises from the first (cubic) anharmonic term of the Taylor expansion of the potential/free energy. Fermi's golden rule yields scattering rates for processes  $\mu \rightarrow \mu' + \mu''$  (phonon splitting, "+") and  $\mu + \mu' \rightarrow \mu''$  (phonon merging, "-"):

$$\Gamma_{\mu\mu'\mu''}^{\pm} = \frac{\hbar\pi}{8\omega_{\mu}\omega_{\mu'}\omega_{\mu''}} |\Phi_{\mu\mu'\mu''}^{\pm}|^2 \Delta_{\mu\mu'\mu''}^{\pm}(n_{\mu'}, n_{\mu''}), \quad (8)$$

where  $\Phi_{\mu\mu'\mu''}^{\pm}$  is the projected third-order potential, and  $\Delta^{\pm}$  encodes energy and momentum conservation, and thermal population factors:

$$\Delta_{\mu\mu'\mu''}^{+} = (n_{\mu'} - n_{\mu''})\delta(\omega_{\mu} - \omega_{\mu'} + \omega_{\mu''})\delta_{\mathbf{q}_{\mu}, \mathbf{q}_{\mu'} - \mathbf{q}_{\mu''} + \mathbf{G}}, \quad (9)$$

$$\Delta_{\mu\mu'\mu''}^{-} = (n_{\mu'} + n_{\mu''} + 1)\delta(\omega_{\mu} + \omega_{\mu'} - \omega_{\mu''})\delta_{\mathbf{q}_{\mu} + \mathbf{q}_{\mu'}, \mathbf{q}_{\mu''} + \mathbf{G}}, \quad (10)$$

with reciprocal lattice vectors  $\mathbf{G}$  allowing umklapp processes that conserve the crystal momentum as in  $\mathbf{q} \pm \mathbf{q}' - \mathbf{q}'' = \mathbf{G}$ . The projected potential is:

$$\Phi_{\mu\mu'\mu''} = \sum_{i\alpha i'\alpha' i''\alpha''} \frac{\phi_{i\alpha i'\alpha' i''\alpha''}'''}{\sqrt{m_i m_{i'} m_{i''}}} \eta_{i\alpha\mu} \eta_{i'\alpha'\mu'} \eta_{i''\alpha''\mu''}, \quad (11)$$

requiring summation over all atoms and Cartesian directions, the most computationally demanding step in ALD calculations. Note that the projected potential is symmetric with respect to the process type:  $\Phi_{\mu\mu'\mu''}^{+} = \Phi_{\mu\mu'\mu''}^{-} \equiv \Phi_{\mu\mu'\mu''}$ , as the same matrix element governs both emission and absorption. The  $\pm$  distinction in Eq. 8 arises solely from the different energy-momentum conservation rules and population factors encoded in  $\Delta^{\pm}$ , not from different interaction strengths. Specifically,  $|\Phi_{\mu\mu'\mu''}^{\pm}|^2$  represents the scattering transition probability, which is intrinsic to the three-phonon interaction and independent of whether the process is absorption or emission.

Energy conservation in the three-phonon scattering processes ( $\omega_{\mu} \pm \omega_{\mu'} - \omega_{\mu''} = 0$ ) is implemented by smearing the frequencies with finite-width distribution functions:

$$\delta(\omega) \approx \frac{1}{\pi} \frac{\sigma/2}{\omega^2 + (\sigma/2)^2} \quad (\text{Lorentzian}), \quad \delta(\omega) \approx \frac{1}{\sqrt{\pi}\sigma} e^{-\omega^2/\sigma^2} \quad (\text{Gaussian}), \quad (12)$$

with bandwidth  $\sigma$  set *via* `third_bandwidth` or calculated adaptively from phonon group velocity dispersions [52]. Both functions are normalized to unity over  $(-\infty, +\infty)$ ; scattering contributions are evaluated only for mode pairs satisfying  $|\Delta\omega| < 2\sigma$ . Three broadening schemes are available via the `broadening_shape` parameter: Lorentzian (`shape='lorentz'`), which has long tails and is exact for exponentially decaying correlations; Gaussian (`shape='gauss'`), the most common choice with smooth and faster-decaying tails; and triangular (`shape='triangle'`), which uses linear interpolation for fast computation at reduced accuracy, suitable for initial screening calculations.

The phonon lifetime (inverse bandwidth) is:

$$\tau_{\mu} = \frac{1}{2\Gamma_{\mu}} = \frac{1}{2\sum_{\mu'\mu''}(\Gamma_{\mu\mu'\mu''}^{+} + \Gamma_{\mu\mu'\mu''}^{-})}. \quad (13)$$

## Computational Implementation

The bottleneck in ALD simulations is calculating phonon coupling terms and scattering matrix elements, which require projecting third-order force constants onto phonon eigenstates (Eq. 11). This projection scales as  $\mathcal{O}((N_q \cdot 3N_b)^3)$ , where  $N_q$  is the number of  $q$ -points.  $\kappa$ ALDo 2.0 implements this algorithm as tensor multiplications:  $N_q \times (3N_b)^2$  for BTE calculations (two  $N_q \times 3N_b$  tensor multiplications). Several optimization strategies are employed:

- **Sparse tensor operations:** Third-order IFCs are stored in coordinate (COO) format and processed using TensorFlow sparse kernels, avoiding dense instantiation.
- **GPU acceleration:** Matrix multiplications in the projection are offloaded to GPU via TensorFlow when available.
- **Selective calculation:** Scattering rates are computed only for physical modes (frequency above `min_frequency`, below `max_frequency`), excluding acoustic modes at  $\Gamma$  and user-defined frequency ranges.
- **Caching:** Intermediate results (`_ps_and_gamma`, `_sparse_phase_and_potential`) are cached to disk in multiple formats (NumPy `.npz`, HDF5), avoiding recomputation in iterative workflows.

The user can control the phonon projection framework through Phonons class parameters: `storage` (memory management strategy), `broadening_shape` (energy conservation kernel), `is_balanced` (symmetrizes population factors in three-phonon scattering rates to enforce detailed balance, improving convergence on coarse  $q$ -grids), and `third_bandwidth` (custom broadening width).

## Thermal Conductivity

Given phonon frequencies, velocities, and scattering rates from the Phonons object, the `Conductivity` class solves for thermal transport using the BTE [64, 38] or the QHGK formalism [41].

### Boltzmann Transport Equation

Under an applied temperature gradient  $\nabla_\alpha T$ , the phonon distribution deviates from equilibrium, with the deviation  $\delta n_\mu$  determined by the linearized BTE:

$$\mathbf{v}_\mu \cdot \nabla T \frac{\partial n_\mu}{\partial T} = - \sum_{\mu'} \tilde{\Gamma}_{\mu\mu'} \delta n_{\mu'}, \quad (14)$$

where the scattering matrix decomposes as  $\tilde{\Gamma}_{\mu\mu'} = \delta_{\mu\mu'} \Gamma_\mu^0 + \Gamma_{\mu\mu'}^1$ , with the diagonal terms calculated as:

$$\Gamma_\mu^0 = \sum_{\mu'\mu''} (\Gamma_{\mu\mu'\mu''}^+ + \Gamma_{\mu\mu'\mu''}^-) \quad (15)$$

and the off-diagonal terms:

$$\Gamma_{\mu\mu'}^1 = - \sum_{\mu''} \left[ \Gamma_{\mu\mu'\mu''}^+ + \Gamma_{\mu\mu'\mu''}^- + \Gamma_{\mu'\mu\mu''}^+ + \Gamma_{\mu'\mu\mu''}^- \right]. \quad (16)$$

that captures mode-coupling. Normal processes ( $\mathbf{G} = 0$ ) redistribute energy without relaxing heat flux, while umklapp processes ( $\mathbf{G} \neq 0$ ) provide thermal resistance.

The BTE can be rewritten as a linear algebra system in which the phonon mean free paths  $\lambda_{\mu'}$  are calculated as:

$$\mathbf{v}_{\mu} = \sum_{\mu'} \left( \delta_{\mu\mu'} \Gamma_{\mu}^0 + \Gamma_{\mu\mu'}^1 \right) \lambda_{\mu'}. \quad (17)$$

The thermal conductivity is then obtained as:

$$\kappa_{\alpha\beta} = \frac{1}{N_q V} \sum_{\mu} c_{\mu} v_{\mu\alpha} \lambda_{\mu\beta}. \quad (18)$$

The phonon mean free paths can be expressed in terms of phonon lifetimes as  $\lambda_{\mu\beta} = v_{\mu\beta} \tau_{\mu\beta}$ . Three solution methods are implemented:

**(i) Relaxation Time Approximation (RTA).** Neglecting off-diagonal coupling ( $\Gamma^1 = 0$ ), the mean free path simplifies to  $\lambda_{\mu\alpha} = \tau_{\mu} v_{\mu\alpha}$  with  $\tau_{\mu} = 1/\Gamma_{\mu}^0$ , yielding:

$$\kappa_{\alpha\beta}^{\text{RTA}} = \frac{1}{N_q V} \sum_{\mu} c_{\mu} v_{\mu\alpha} \tau_{\mu} v_{\mu\beta} = \frac{1}{N_q V} \sum_{\mu} c_{\mu} v_{\mu\alpha} \frac{1}{\Gamma_{\mu}^0} v_{\mu\beta}. \quad (19)$$

This approximation neglects momentum-conserving normal (N) processes. Whereas it is usually sufficiently accurate for systems with strong Umklapp scattering, it may underestimate the thermal conductivity by more than 50% in materials where N-processes are significant [65].

**(ii) Self-Consistent Iterative Method (SC).** The full BTE (Eq. 17) is solved iteratively [66, 67]:

$$\lambda_{\mu\alpha}^{(n+1)} = \frac{v_{\mu\alpha}}{\Gamma_{\mu}^0} - \frac{1}{\Gamma_{\mu}^0} \sum_{\mu'} \Gamma_{\mu\mu'}^1 \lambda_{\mu'\alpha}^{(n)}, \quad (20)$$

initialized with RTA solution  $\lambda_{\mu\alpha}^{(0)} = v_{\mu\alpha}/\Gamma_{\mu}^0$ . Convergence is guaranteed when  $\|\Gamma^1/\Gamma^0\| < 1$  [68]. The user specifies the maximum number of iterations (`n_iterations`) and convergence tolerance (`tolerance`) on the relative change in the isotropically-averaged thermal conductivity:  $|\kappa^{(n+1)} - \kappa^{(n)}|/\kappa^{(n)} < \epsilon_{\text{tol}}$  between successive iterations, where  $\kappa = \text{Tr}(\kappa_{\alpha\beta})/3$ . This method balances accuracy and memory, avoiding explicit storage of the full scattering matrix.

**(iii) Full Matrix Inversion.** The exact solution of Eq. 17 can be obtained by inverting the scattering matrix.

$$\kappa_{\alpha\beta} = \frac{1}{N_q V} \sum_{\mu\mu'} c_{\mu} v_{\mu\alpha} (\tilde{\Gamma}^{-1})_{\mu\mu'} v_{\mu'\beta}. \quad (21)$$

This provides the most accurate BTE solution but requires storing the full  $(N_q \cdot 3N) \times (N_q \cdot 3N)$  scattering matrix, limiting applicability to moderate system sizes.

Method selection is specified via `method='rta'/'sc'/'inverse'/'full'` when instantiating the Conductivity object. Memory scaling differs significantly: RTA and self-consistent methods require  $N_q \times (3N)^2$  storage, while full inversion and eigendecomposition require  $(N_q \cdot 3N)^2$  storage. For most bulk materials at moderate temperatures, the self-consistent method provides an optimal balance of accuracy and computational cost, while RTA is suitable for quick estimates and materials with strong anharmonicity.

**Finite-size effects, boundary scattering, and eigendecomposition approach.** When characteristic sample dimensions  $L_{\alpha}$  become comparable to or smaller than phonon mean free paths,

confinement and boundary scattering fundamentally alter thermal transport [69, 70]. This regime is ubiquitous in nanoscale systems, including nanowires, thin films, superlattices, and nanostructured thermoelectrics, as well as in low-dimensional materials (graphene, nanotubes) at cryogenic temperatures, where thermal phonon mean free paths can exceed millimeters [71].

`κALDo 2.0` provides two complementary approaches to address finite-size transport. The first adds a boundary scattering term to the diagonal of the full scattering matrix before inversion [72, 73]:

$$\tilde{\Gamma}_{\mu\mu'}^{\text{fs}} = \tilde{\Gamma}_{\mu\mu'} + \delta_{\mu\mu'} \frac{2|v_{\mu\alpha}|}{L_\alpha}, \quad (22)$$

where  $v_{\mu\alpha}$  is the group velocity component and  $L_\alpha$  the sample dimension along direction  $\alpha$ . The mean free path is then obtained from full matrix inversion:

$$\lambda_{\mu\alpha}^{\text{fs}} = \sum_{\mu'} [(\tilde{\Gamma}^{\text{fs}})^{-1}]_{\mu\mu'} v_{\mu'\alpha}. \quad (23)$$

Unlike Matthiessen's rule, which would simply add scattering rates for independent modes ( $\tau_{\text{eff}}^{-1} = \tau_{\text{anh}}^{-1} + 2|v|/L$ ), this formulation preserves the off-diagonal scattering matrix elements  $\Gamma_{\mu\mu'}^1$  that describe momentum exchange between modes, correctly capturing the interplay between boundary scattering and collective phonon transport. This is selected via `finite_length_method='ms'`, with sample dimensions specified via `length=(L_x, L_y, L_z)` in Ångströms (using `None` or `0` for infinite dimensions). For strongly confined systems with  $L \ll \lambda_{\text{ph}}$ , the ballistic limit (`finite_length_method='ballistic'`) is also available.

The second approach employs full eigendecomposition of the scattering matrix (`method='full'`) [68]. The method diagonalizes the scattering matrix  $\Gamma = U\Lambda U^T$ , where  $\Gamma$  is the  $(N_q \cdot 3N) \times (N_q \cdot 3N)$  phonon-phonon scattering matrix,  $U$  contains the eigenvectors (columns), and  $\Lambda$  is a diagonal matrix of eigenvalues representing the decay rates of the collective heat-carrying excitations (termed "relaxons" in the original formulation). These collective modes decay exponentially as  $e^{-\lambda_i t}$  with time constants  $\tau_i = 1/\lambda_i$ , where  $\lambda_i$  are the eigenvalues. Rather than treating each phonon mode independently as in RTA, this approach identifies the true collective eigenmodes of the scattering operator that carry heat. This is essential in the hydrodynamic regime where momentum-conserving normal (N) processes dominate, causing breakdown of conventional RTA and self-consistent approximations. The eigendecomposition enables mode-by-mode analysis of transport contributions through the eigenvalue spectrum and can filter unphysical negative eigenvalues via `is_using_gamma_tensor_evects`, improving numerical stability. For a detailed description of the formalism and its physical interpretation, see Ref. [68, 74].

## Quasi-Harmonic Green-Kubo (QH GK)

The QH GK approach [41] provides a unified lattice dynamic theory for both crystalline and disordered systems. This theory bridges and extends the BTE method for crystals and the Allen-Feldman theory for glasses [75, 76], and results in equations practically equivalent to the Wigner transport formalism [40, 77], naturally capturing diffusion and locon contributions [78, 43] (vibrational modes that transport heat through diffusion or remain localized, respectively).

The QH GK approach is particularly relevant for disordered, defective, and amorphous materials, where translational symmetry is broken, and the traditional BTE framework (which relies on well-defined wavevectors and Bloch states) becomes inapplicable, and for strongly anharmonic crystals

for which the interband contribution to heat transport is substantial. For amorphous systems, QHGK is formulated as a real-space,  $\Gamma$ -point approach for large simulation cells ( $N_q = 1$ , large  $N$ ), using  $(3N)^2$  storage to save the system state, making it computationally efficient for modeling disorder at the atomic scale. The thermal conductivity is:

$$\kappa_{\alpha\beta} = \frac{1}{V} \sum_{\mu\mu'} c_{\mu\mu'} v_{\mu\mu'}^\alpha \tau_{\mu\mu'} v_{\mu\mu'}^\beta, \quad (24)$$

where  $c_{\mu\mu'}$  are generalized modal heat capacities defined as  $c_{\mu\mu'} = \frac{k_B}{T} \frac{\omega_\mu \omega_{\mu'} (n_\mu - n_{\mu'})}{\omega_{\mu'} - \omega_\mu}$  for  $\mu \neq \mu'$  and  $c_{\mu\mu} = c_\mu$  (the diagonal heat capacity from Eq. 7) for degenerate modes. The generalized velocities are defined as  $v_{\mu\mu'}^\alpha = \sum_{i\beta i'\beta'} \eta_{i\beta\mu}^* \frac{\partial D_{i\beta i'\beta'}}{\partial R_{i'\alpha}} \eta_{i'\beta'\mu'}$ , where  $\partial D / \partial R_{i'\alpha}$  represents the derivative of the dynamical matrix with respect to atomic position, capturing how vibrational modes couple through atomic displacements. This operator captures non-diagonal contributions arising from the breakdown of wavevector definition in disordered systems, essential for representing diffuson transport. The generalized lifetimes  $\tau_{\mu\mu'}$  are computed from thermal diffusivities with a broadening function. For Lorentzian broadening,

$$\tau_{\mu\mu'} = \frac{\gamma_{\mu\mu'}}{2[(\omega_\mu - \omega_{\mu'})^2 + \gamma_{\mu\mu'}^2]}, \quad (25)$$

where  $\gamma_{\mu\mu'}$  is the bandwidth parameter controlling the energy resolution.

However, the impact of QHGK is not limited to disordered systems. Indeed, in crystals, the QHGK approach highlights an additional transport contribution on top of the BTE one. In the RTA, it reads:

$$\kappa_{\alpha\beta} = \kappa^{\text{RTA}} + \frac{1}{V} \sum_{\mathbf{q}s \neq \mathbf{q}'s'} c_{\mathbf{q}s s'} v_{\mathbf{q}s s'}^\alpha \tau_{\mathbf{q}s s'} v_{\mathbf{q}s s'}^\beta, \quad (26)$$

where phonon is explicitly labeled with its own Bloch wavevector  $\mathbf{q}$  and band index  $s$ ,  $\mu = (\mathbf{q}s)$ . The second sum in the expression indicated the so-called interband contribution [40], between pairs of phonons with the same wavevector but different band indices. Although the BTE is generally dominant for most crystals, it has been shown that the additional term can significantly affect the thermal conductivity and its temperature dependence in certain crystals, e.g., GeTe and halide perovskites [79, 44]. Finally, the QHGK formalism can be further extended beyond the RTA by employing the full scattering matrix in the intraband term [40, 77]. In practice,  $\kappa^{\text{RTA}}$  is replaced by the full BTE result, while the interband contribution is retained at the RTA level. As shown in Ref. [77], the full scattering matrix is typically relevant only at very low temperatures, where the interband contribution becomes negligible, thereby justifying the simplified RTA treatment adopted for the latter.

In addition to thermal conductivity, the QHGK method computes mode-resolved thermal diffusivities  $D_\mu$  accessible via `Conductivity.diffusivity`, providing insight into the spatial extent of vibrational energy transport and enabling identification of propagons, diffusons, and locons in disordered materials. Implementation details follow Ref. [41], with broadening controlled by `diffusivity_bandwidth` and `diffusivity_shape` (Lorentzian, Gaussian, or triangular kernels).

## Modeling Extensions

Beyond core thermal conductivity calculations,  $\kappa$ ALDo 2.0 provides specialized capabilities for challenging materials and computational efficiency enhancements for large-scale studies.

## Isotopic Scattering

Natural isotopic disorder introduces mass variance that scatters phonons even in otherwise perfect harmonic crystals. Following Tamura’s perturbation theory [80], the isotopic scattering rate for a phonon mode  $(\mathbf{q}, s)$  reads

$$\gamma_{\mathbf{q}s}^{\text{iso}} = \frac{\pi}{2N_q} \omega_{\mathbf{q}s}^2 \sum_{\mathbf{q}'s'} \delta(\omega_{\mathbf{q}s} - \omega_{\mathbf{q}'s'}) \sum_{i\alpha} g_i \left| \eta_{\mathbf{q}s}^{*,i\alpha} \eta_{\mathbf{q}'s'}^{i\alpha} \right|^2, \quad (27)$$

where  $\mathbf{q}$  and  $s$  denote the phonon wavevector and band index, respectively,  $\alpha$  labels the Cartesian direction, and  $g_i = \sum_{\text{iso}} f_{i,\text{iso}} (\Delta M_{i,\text{iso}}/M_i)^2$  is the relative mass-variance parameter of the  $i$ -th atom in the unit cell, defined in terms of the isotope fraction  $f_{i,\text{iso}}$  and mass deviation  $\Delta M_{i,\text{iso}}$ . In practice, isotopic scattering can be enabled by setting `include_isotopes=True`. If the input `g_factor` array is omitted, natural isotopic abundances from the ASE database are automatically used to compute it. Moreover, by tuning the `g_factor`, Tamura’s formalism provides a perturbative description of mass-disorder scattering in alloyed systems, such as silicon–germanium alloys [81, 46].

Finally, the total scattering rate becomes  $\gamma_\mu = \gamma_\mu^{\text{anh}} + \gamma_\mu^{\text{iso}}$ .

## Non-Analytical Term Corrections

In polar materials (ionic or covalent crystals with non-zero Born effective charges), long-range dipole-dipole interactions render the dynamical matrix non-analytic at  $\Gamma$  [82]. This causes directional dependence of the longitudinal optical (LO) and transverse optical (TO) mode splitting in the  $\mathbf{q} \rightarrow 0$  limit. Neglecting this effect produces incorrect phonon dispersions near  $\Gamma$  and erroneous thermal conductivities.

`κALDo 2.0` implements the non-analytical correction (NAC) following Gonze and Lee:

$$D_{i\alpha i'\beta}^{\text{NAC}}(\mathbf{q}) = \frac{1}{\sqrt{m_i m_{i'}}} \frac{4\pi}{V_{\text{cell}}} \frac{(\sum_\gamma q_\gamma Z_{i,\gamma\alpha}^*) (\sum_{\gamma'} q_{\gamma'} Z_{i',\gamma\beta}^*)}{\sum_{\alpha\beta} q_\alpha \epsilon_{\alpha\beta}^\infty q_\beta}, \quad (28)$$

where  $Z_{i,\gamma\alpha}^*$  is the Born effective charge tensor and  $\epsilon_{\alpha\beta}^\infty$  the high-frequency dielectric tensor. These quantities are obtained from DFPT calculations (Quantum ESPRESSO’s `ph.x`) and imported via the `is_nac=True` flag during Phonons initialization. The NAC term is added to  $D(\mathbf{q})$  before diagonalization for all  $\mathbf{q}$  near  $\Gamma$ . Figure 9 in Section 3 demonstrates the importance of NAC for polar oxides.

## Low-Dimensional Systems: Nanowires and Nanotubes

`κALDo 2.0` provides specialized support for quasi-one-dimensional systems such as nanowires and carbon nanotubes via the `is_nw` flag. In these geometries, translational symmetry is broken in two directions while periodic boundary conditions apply along the transport axis. Setting `is_nw=True` modifies the  $k$ -point sampling strategy to focus computational effort along the transport direction (e.g., `kpts=[1, 1, 11]` for  $z$ -axis transport), and adjusts the thermal conductivity normalization to account for the reduced cross-sectional area rather than three-dimensional volume.

This capability is particularly valuable for studying thermal transport in carbon nanotubes, semiconductor nanowires, and other quasi-1D structures [where boundary scattering and reduced dimensionality dominate](#). When combined with finite-size effects (length parameter), `κALDo 2.0`

enables prediction of length-dependent thermal conductivity in nanotubes and nanowires, critical for thermoelectric and thermal interface material applications [83].

## Elastic Properties

The same second-order force constants used for phonon calculations also determine elastic properties. The elastic stiffness tensor  $C_{ijkl}$  relates stress and strain via generalized Hooke's law. Following the derivation in Ref. [84], the elastic tensor is computed from:

$$C_{ijkl} = \frac{1}{V} \left[ \sum_{nm} \phi_{nm,ik,jl}^{(2)} + \sum_{n\mu} \frac{(\partial D / \partial \varepsilon_{ij})_{n\mu} (\partial D / \partial \varepsilon_{kl})_{n\mu}}{\omega_{\mu}^2} \right], \quad (29)$$

where indices  $i, j, k, l$  denote Cartesian directions and strain components, and  $\varepsilon$  is the strain tensor. The implementation in `ForceConstants.elastic_prop()` returns the full fourth-rank tensor in GPa. Derived quantities, like the bulk modulus  $B$ , shear modulus  $G$ , and Young's modulus  $E$ , are extracted using Voigt-Reuss-Hill averaging. This capability is particularly valuable when combined with TDEP, enabling temperature-dependent elastic constant determination from the same MD trajectories used for thermal conductivity [51].

## Harmonic Free Energy and Thermal Expansion via Quasi-Harmonic Approximation

$\kappa$ ALDo 2.0 implements calculation of the harmonic contribution to the Helmholtz free energy for a system of harmonic oscillators with frequencies  $\omega_{\mu}(\mathbf{q})$ :

$$F_{\text{vib}}(T) = \sum_{\mathbf{q}\mu} \left[ \frac{\hbar\omega_{\mu}(\mathbf{q})}{2} + k_B T \ln \left( 1 - e^{-\hbar\omega_{\mu}(\mathbf{q})/(k_B T)} \right) \right], \quad (30)$$

which includes both the zero-point energy contribution and the thermal population term. This quantity is essential for thermodynamic calculations and enables thermal expansion predictions via the quasi-harmonic approximation (QHA) [85, 86, 87].

In the QHA framework, temperature-dependent equilibrium volumes and elastic properties are determined by minimizing the total Helmholtz free energy:

$$F(V, T) = E_0(V) + F_{\text{vib}}(V, T) = E_0(V) + \sum_{\mu} \left[ \frac{\hbar\omega_{\mu}(V)}{2} + k_B T \ln \left( 1 - e^{-\hbar\omega_{\mu}(V)/(k_B T)} \right) \right], \quad (31)$$

where  $E_0(V)$  is the static lattice energy and  $F_{\text{vib}}(V, T)$  is the vibrational free energy evaluated at different volumes. By calculating force constants and phonon frequencies across a grid of lattice parameters (controlled via the `quasiharmonic` module), the code determines equilibrium volumes, thermal expansion coefficients  $\alpha(T) = (1/V)(\partial V / \partial T)_P$ , and pressure-temperature phase diagrams. This functionality complements TDEP workflows by providing an alternative route to finite-temperature lattice properties when the computational cost of systematic volume sampling is acceptable. QHA is particularly useful for materials with moderate anharmonicity where explicit inclusion of temperature-dependent force renormalization (via TDEP) may not be necessary.

## Analysis Tools

### Anharmonicity Quantification

Before devoting to expensive thermal transport calculations, it is useful to assess whether anharmonicity is significant. The  $\sigma_A$  score [88] represents anharmonic strength by comparing actual forces to their anharmonic contributions:

$$\sigma_A = \sqrt{\frac{\langle (F^{\text{anharm}})^2 \rangle}{\langle F^2 \rangle}}, \quad F^{\text{anharm}} = F - F^{\text{harm}}, \quad (32)$$

where  $F$  are forces along an MD trajectory and  $F^{\text{harm}} = -\Phi^{(2)} \cdot u$  are forces predicted from second-order IFCs and displacements  $u$ .  $\sigma_A$  below 0.1 indicates a harmonic regime,  $0.1 < \sigma_A < 0.5$  for weak anharmonicity, and  $\sigma_A$  greater than 0.5 signifies strong anharmonicity, which indicates that accurate lattice thermal conductivity predictions might require beyond three-phonon BTE or molecular dynamics. The function `sigma2_tdep_md()` in the `controllers.sigma2` module automates this calculation given TDEP force constants and an MD trajectory.

### Participation Ratio

The participation ratio  $PR_\mu$  quantifies mode localization, particularly important in disordered systems:

$$PR_\mu = \frac{1}{N} \left( \sum_{i=1}^N \sum_{\alpha} |\eta_{i\alpha\mu}|^2 \right)^2 \left( \sum_{i=1}^N \sum_{\alpha} |\eta_{i\alpha\mu}|^4 \right)^{-1}. \quad (33)$$

Extended modes have  $PR \sim 1$ , while localized modes have  $PR \ll 1$  [78]. Computed automatically via `Phonons.participation_ratio`, this property helps identify diffuson and locon contributions to thermal conductivity.

## Software Architecture and Performance

### Object-Oriented Design and Lazy Evaluation

`κALDo 2.0` employs a three-tier class hierarchy mirroring the computational workflow: `ForceConstants` manages IFCs and atomic geometry, `Phonons` computes vibrational properties and scattering rates, and `Conductivity` solves the BTE or QHGK. Each class inherits from the `Storable` base class, implementing lazy evaluation via the `@lazy_property` decorator pattern. Expensive properties (e.g., scattering rates, mean free paths) are computed only when accessed and cached automatically based on a label encoding relevant parameters (temperature,  $q$ -mesh, statistics). This dramatically reduces computation time for iterative workflows like convergence testing and parameter sweeps.

### Storage Backends

Four storage formats accommodate different use cases, selected via `storage='formatted'/'numpy'/'hdf5'/'memory'`: `formatted` text files enable human inspection and interoperability; binary NumPy arrays provide fast I/O for production calculations; HDF5 organizes

complex multi-parameter datasets; and memory-only mode suits transient calculations. Table 2 provides detailed performance characteristics.

**Table 2** Comparison of storage backends for caching intermediate results in  $\kappa$ ALDo 2.0 calculations.

Backend	I/O Speed	Storage Efficiency	Recommended Use Case
formatted	Slow (text parsing)	Low (ASCII)	Human inspection; small systems; sharing with non-Python tools
numpy	Fast (binary)	High (compressed)	Production calculations; large systems; iterative workflows
hdf5	Fast (binary)	High (compressed)	Complex datasets; multiple parameter sets; database integration
memory	Fastest (RAM only)	N/A (no disk)	Transient calculations; HPC job arrays; testing

## Visualization and Analysis Tools

$\kappa$ ALDo 2.0 includes comprehensive plotting utilities via the `plotter` module for rapid visualization and analysis of phonon properties. The `plot_crystal()` function automatically generates publication-quality figures for crystalline materials including: (i) phonon dispersion along high-symmetry paths, (ii) phonon density of states, (iii) group velocity versus  $q$ -vector, (iv) group velocity versus frequency, (v) heat capacity versus frequency, (vi) three-phonon scattering phase space, (vii) phonon lifetimes, (viii) scattering rates, (ix) mean free paths, (x) per-mode thermal conductivity contributions, (xi) cumulative  $\kappa$  versus frequency, and (xii) cumulative  $\kappa$  versus mean free path. For disordered and amorphous systems, `plot_amorphous()` provides all frequency-dependent plots plus mode thermal diffusivity and participation ratio analyses, essential for identifying propagons, diffusons, and locons. Individual plotting functions (`plot_dispersion()`, `plot_dos()`, `plot_vs_frequency()`) enable custom analysis workflows. All figures are automatically saved in high resolution with systematic folder organization based on simulation parameters (temperature,  $q$ -mesh, solution method), facilitating comparison across parameter sets.

## Performance Optimization

Key performance features include:

**Sparse tensor operations:** Third-order IFCs and scattering matrices are stored and manipulated in sparse formats (COO, CSR), reducing memory footprint by 100–1000 $\times$  for typical systems.

**GPU acceleration:** TensorFlow backend automatically utilizes available GPUs for tensor contractions in the IFC projection step (Eq. 11). Benchmarks on NVIDIA A100 show 5–10 $\times$  speedup relative to CPU for  $N > 50$  atom unit cells. Further benchmark of runtime as a function of system sizes is shown in Figure 3.

**Multi-temperature optimization:** Version 2.0 decouples temperature-invariant computations from temperature-dependent population factors, enabling efficient thermal conductivity calculations across multiple temperatures. The computationally intensive projection of third-order force constants

onto phonon modes (Eq. 11) is decoupled from temperature-dependent population factors. This allows the projection tensors to be computed once and cached, reducing the complexity of subsequent temperature sweeps from  $\mathcal{O}(N_T \cdot N^3)$  to  $\mathcal{O}(N^3 + N_T \cdot N^2)$ , where  $N_T$  is the number of temperatures, providing order-of-magnitude speedups for typical material screening workflows.

**Vectorization:** NumPy broadcasting and `opt_einsum` optimized contractions minimize Python-level loops in scattering calculations.

**Parallel  $q$ -point loops:** Phonon property calculations at different  $q$ -points are embarrassingly parallel. While the current implementation is serial, users can easily parallelize via external job managers (SLURM array jobs, Python multiprocessing).

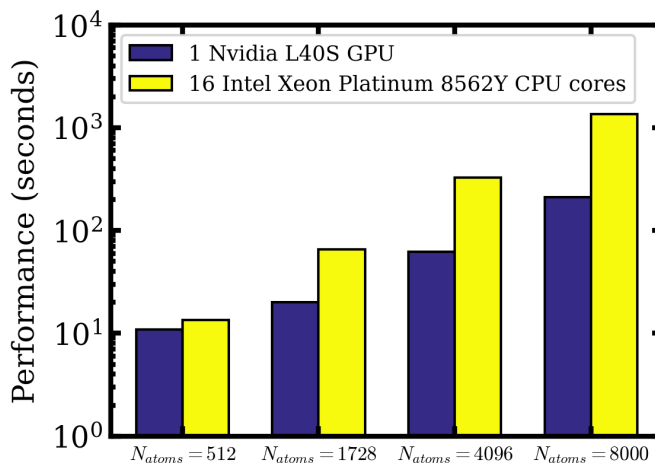


**Figure 3** Runtime profiling was performed for QHGK calculations of the lattice thermal conductivity of bulk Si across a range of system sizes, using a fixed  $3 \times 3 \times 3$   $q$ -grid. Benchmarks were run on a single NVIDIA L40S GPU and on 16 CPU cores of an Intel Xeon Platinum 8562Y processor. Interatomic force constants for the profiling were obtained using the Tersoff potential.[89]

## Deployment and Documentation

$\kappa$ ALDo 2.0 emphasizes reproducibility and accessibility:

**Containerization:** Docker images with all dependencies pre-installed enable one-line deployment across platforms.

**Cloud tutorials:** Google Colab notebooks provide interactive tutorials runnable in web browsers without local installation.

**Continuous integration:** Automated testing via CircleCI ensures code quality. Pull requests require passing 40+ unit tests covering core functionality and regression prevention.

**Auto-generated documentation:** Sphinx processes docstrings into HTML/PDF manuals hosted at <https://nanotechnologygroup.github.io/kaldo>, synchronized with each release.

**Example library:** A standalone repository hosted at <https://github.com/nanotechnologygroup/kaldo-examples> containing detailed examples to model lattice thermal conductivity of semiconducting materials (e.g. Si, Ge, SiC, GaAs, MgO, AlN, NaCl) using various workflows including DFT with

DFPT/D3Q, empirical potentials via LAMMPS, and machine-learned potentials (MatterSim [24], ORB [25], NEP [21], ACE [51], UPET [90]).

## Example: Basic Workflow

To illustrate typical usage, we present an example calculating the thermal conductivity of SiC using the MatterSim machine-learned potential with structure optimization:

```
1 # Import kALDo classes and ASE
2 from kaldo.forceconstants import ForceConstants
3 from kaldo.phonons import Phonons
4 from kaldo.conductivity import Conductivity
5 import kaldo.controllers.plotter as plotter
6 from ase.build import bulk
7 from ase.optimize import BFGS
8 from ase.constraints import StrainFilter
9 from mattersim.forcefield import MatterSimCalculator
10
11 # Stage 1: Structure optimization
12 atoms = bulk('SiC', 'zincblende', a=4.35)
13 calc = MatterSimCalculator(device='cuda')
14 atoms.calc = calc
15
16 # Optimize lattice parameters and atomic positions
17 sf = StrainFilter(atoms)
18 opt = BFGS(sf)
19 opt.run(fmax=0.001)
20
21 # Stage 2: Compute force constants using finite differences
22 fc = ForceConstants(
23     atoms=atoms,
24     supercell=[10, 10, 10],
25     third_supercell=[5, 5, 5],
26     folder='fd_SiC_MatterSim'
27 )
28 fc.second.calculate(calc, delta_shift=0.03)
29 fc.third.calculate(calc, delta_shift=0.03)
30
31 # Stage 3: Calculate phonon properties
32 phonons = Phonons(
33     forceconstants=fc,
34     kpts=[15, 15, 15],
35     temperature=300,
36     is_classic=False,
37     folder='ALD_SiC_MatterSim'
38 )
39
40 # Plot phonon dispersion
41 plotter.plot_dispersion(phonons, n_k_points=300)
42
43 # Stage 4: Calculate thermal conductivity
44 cond = Conductivity(phonons=phonons, method='inverse')
45
46 # Access results
47 kappa = cond.conductivity.sum(axis=0)
```

```
48 print(f"Thermal conductivity: {kappa.trace()/3:.1f} W/m/K")
```

More complex workflows involving TDEP, isotopic scattering, or NAC corrections follow this same pattern with additional keyword arguments documented in the API reference.

## Command-Line Interface

$\kappa$ ALDo 2.0 includes a command-line interface (`kaldo/cli/`) that accepts JSON-formatted configuration files, simplifying deployment on clusters and HPC systems. This declarative approach is particularly useful for batch job submission, parameter sweeps, and reproducible workflows where separating calculation parameters from execution logic is beneficial. A typical configuration file specifies the force constants, phonon calculation parameters, conductivity method, and optional visualization settings. While the Python API offers maximum flexibility for power users and complex research workflows, the JSON interface is optimized for high-throughput batch processing on HPC resources.

```
{
  "description": "Example kALDo configuration using silicon crystal test data",
  "forceconstants": {
    "folder": "kaldo/tests/si-crystal",
    "format": "eskm",
    "supercell": [3, 3, 3]
  },
  "phonons": {
    "temperature": 300.0,
    "kpts": [5, 5, 5],
    "is_classic": false,
    "storage": "memory"
  },
  "conductivity": {
    "method": "rta",
    "storage": "memory"
  },
  "plotter": {
    "plot_dispersion": {
      "n_k_points": 300,
      "is_showing": false,
      "with_velocity": true,
      "folder": "plots"
    }
  }
}
```

The configuration is executed via `kaldo < example.in`, making it ideal for automated workflows and ensuring complete reproducibility of calculations.

# Applications

We demonstrate  $\kappa$ ALDo 2.0’s advanced capabilities through case studies of two prototypical materials: the halide perovskite  $\text{CsPbBr}_3$  and the polar oxide MgO. These examples showcase the software’s key features, including TDEP-based temperature-dependent force constants for materials with strong anharmonicity ( $\text{CsPbBr}_3$ ), non-analytical corrections for polar materials (MgO), and seamless integration with machine-learned potentials (MatterSim) and electronic structure package (d3q). Together, these applications illustrate how  $\kappa$ ALDo 2.0 addresses challenging materials where conventional harmonic approaches fail, while providing the flexibility to combine multiple computational methods (DFPT, MLPs, TDEP) within a unified workflow.

## Cubic $\text{CsPbBr}_3$ using TDEP

To study the cubic phase of  $\text{CsPbBr}_3$ , we employ the temperature-dependent effective potential (TDEP) methodology. Experimentally,  $\text{CsPbBr}_3$  transforms into the  $Pm\bar{3}m$  phase above approximately 411 K, where anharmonic lattice dynamics play a central role in stabilizing the structure. Within the harmonic approximation, the cubic phase is dynamically unstable due to soft phonon modes at the  $M$  and  $R$  points. By fitting temperature-dependent interatomic force constants from classical molecular dynamics trajectories, TDEP provides renormalized phonon dispersions that recover phase stability and enable a quantitative description of vibrational and thermal transport properties. In this phase,  $\text{CsPbBr}_3$  exhibits the highest lattice thermal conductivity among its polymorphs, although phonon spectral functions show strongly overdamped, non-Lorentzian lineshapes that signal intense anharmonicity.

To perform this calculation, we run an NPT equilibration step on a  $6\times 6\times 6$  cubic  $\text{CsPbBr}_3$  supercell followed by an NVT simulation in GPUMD using a NEP potential developed by Erik Fransson et al[91]. We sample 200 frames evenly from the trajectory and fit the TDEP second- and third-order interatomic force constants to the chosen frames. Thermal conductivity is then calculated on a  $12\times 12\times 12$   $q$ -grid. Non-analytical corrections are not applied in this example, as the LO–TO splitting is negligible in  $\text{CsPbBr}_3$  and has no effect on  $\kappa$  [92].

In Fig. 4, the phonon dispersion relations capture the phonon mode softening at the  $M$  and  $R$  points as the phase transition of the potential is approached from above ( $\approx 340$  K). The total impact of coherent transport is determined by calculating the interband phonon contribution to the thermal conductivity using Eq. 26, which gives the relation [77]:

$$\kappa_T = \kappa_{inv} + (\kappa_{QHGK} - \kappa_{RTA}) \quad (34)$$

Interband transport contributions are present and account for  $\approx 25\%$  of total thermal conductivity in Fig 5, but they are relatively weaker than in the lower-symmetry tetragonal and orthorhombic phases, in line with experimental evidence of anomalous heat conduction in this material.

Lastly, we plot various properties related to the second and third order interatomic force constants in Fig. 6 and Fig. 7 to gauge the impact of finite temperature renormalization on them. We notice little impact on increasing temperature on second order properties from 360 K to 500 K, however, third order properties change much more dramatically, with a scattering phase space increase of  $\approx 60\%$  and consistently larger lifetimes at 360 K compared to 500 K by about 1 order of magnitude.

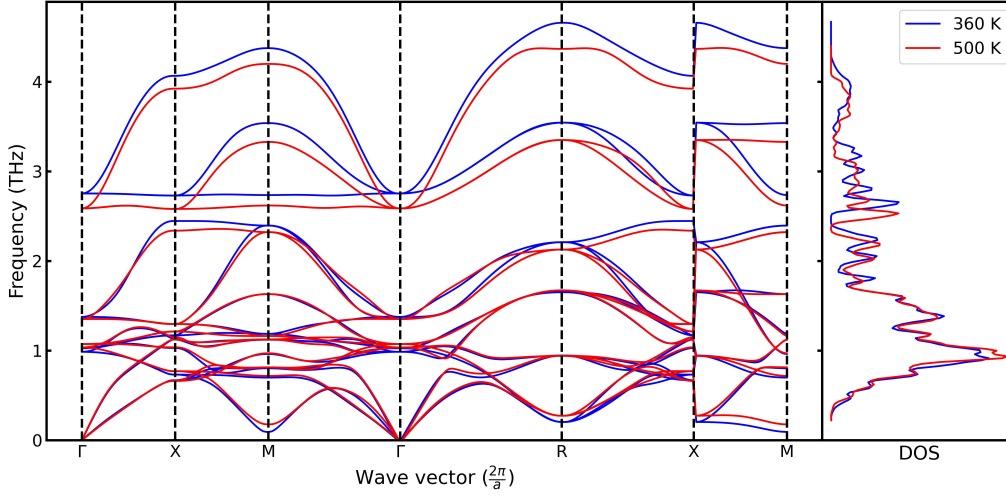


**Figure 4** Phonon dispersion relation (left) and density of states (right) for cubic phase  $\text{CsPbBr}_3$  at 360 and 500 K.

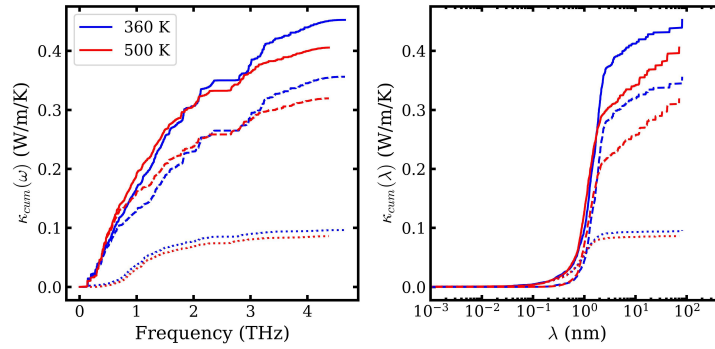


**Figure 5** Cumulative thermal conductivity with respect to phonon mode frequency (left) and phonon mean free path (right). Dashed lines are used to indicate coherent contribution from QHGK, dotted lines are used to indicate the BTE contribution, and solid lines indicate total thermal conductivity calculated by adding the coherent (diffuson) contribution, estimated as the difference between the full QHGK and RTA, to the exact BTE solution ( $\kappa_{inv}$ ).

## Thermal Properties of MgO: QHA Thermal Expansion and NAC Corrections

To test our new free energy calculator and quasiharmonic algorithm, we perform the quasiharmonic approximation on MgO from 0 to 900 K using the MatterSim potential developed using PBE level of theory on a  $3 \times 3 \times 3$  supercell and  $12 \times 12 \times 12$   $q$ -grid using 21 evenly spaced lattice constants between 4.23027 and 4.35846 Å. The resulting free energy, lattice constant, and volumetric thermal

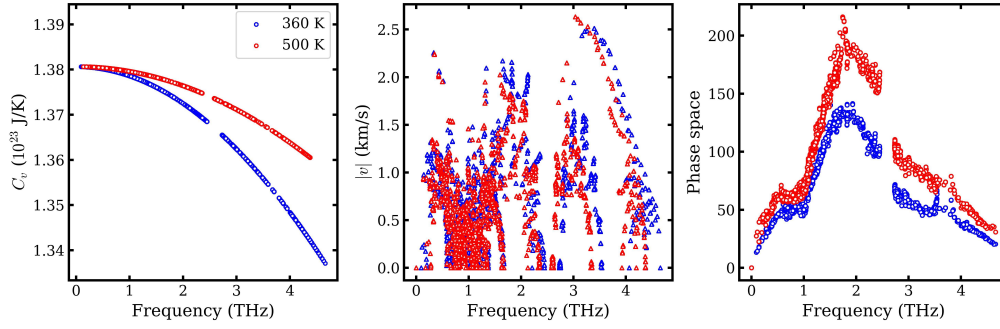


**Figure 6** Phonon heat capacity (left), group velocity magnitude (middle), and scattering phase space (right) for 360 and 500 K cubic CsPbBr<sub>3</sub>.

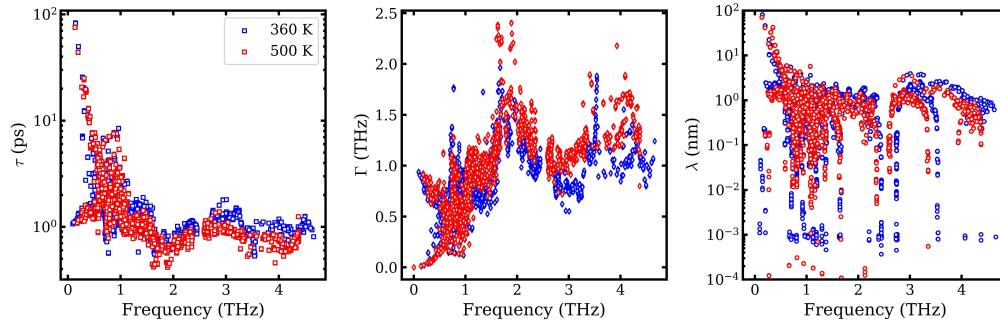


**Figure 7** Phonon lifetimes (left), scattering rate (middle), and mean free path (right) for 360 and 500 K cubic CsPbBr<sub>3</sub>.

expansion are shown below in Fig. 8.

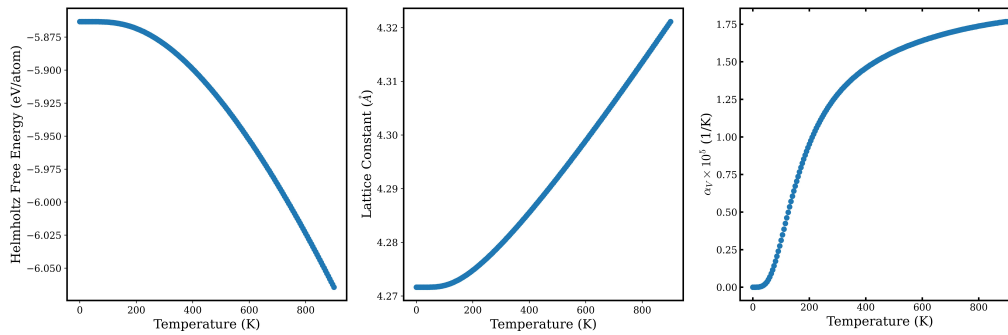


**Figure 8** Quasiharmonic calculation performed on cubic phase MgO using MatterSim machine learned potential.

Lattice dynamics calculations were carried out on rock-salt MgO at 300 K to assess the role of

long-range Coulomb interactions on the thermal transport of a polar material. The second- and third-order force constants are obtained with DFPT[93, 57] using the norm-conserving Vanderbilt pseudopotentials for Mg and O[94]. Figure 9 shows the phonon frequency dispersion with and without the inclusion of non-analytical corrections (NAC)[82]. Near  $\Gamma$ , the longitudinal-optical (LO) branch is hardened, opening a clear LO–TO split, while leaving the acoustic branches unchanged. This shift leads to a small suppression in the thermal conductivity, primarily through the diminished contribution of optical phonons as seen in the plot of the cumulative  $\kappa$  ( $\kappa_{cum}$ ) against frequency in Figure 10. The cumulative thermal conductivity  $\kappa_{cum}$  exhibits a steeper initial rise and converges to a higher value without NAC ( $\sim 5$  W/m/K higher), indicating that optical and mid-frequency acoustic modes are over-contributing when the LO–TO splitting is neglected. The reduction occurs primarily through reduced mode velocities, as the lifetimes are almost identical.

The  $\kappa$  of both systems was measured across a broad temperature span in Figure 11. Thermal conductivity falls proportionally with  $T^{-1}$  for both calculations at low temperature, consistent with Umklapp-dominated transport. The NAC curve stays systematically lower than the result without corrections across the entire range. The gap is largest at low temperature, where long-lived optical modes have the highest impact. The gap slowly narrows at high-T as strong phonon–phonon scattering washes out details of the spectrum.

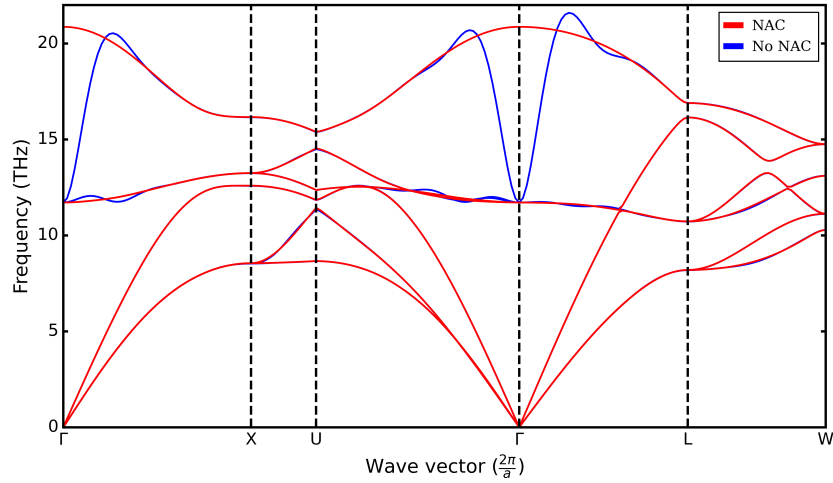


**Figure 9** The phonon dispersion of MgO along a high symmetry path with (red) and without (blue) the NAC correction.

## Conclusions and Outlook

We have presented  $\kappa$ ALDo v2.0, a comprehensive open-source platform for thermal transport calculations from anharmonic lattice dynamics. The software provides researchers with a unified framework combining (i) flexible force constant import from DFT, empirical potentials, and machine-learned potentials, (ii) efficient implementations of BTE (RTA, self-consistent, full inversion) and

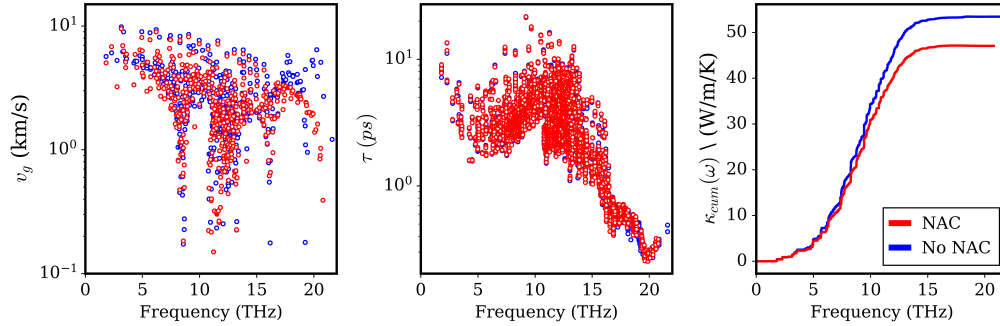


**Figure 10** Phonon velocities (left), lifetimes (middle), and cumulative thermal conductivity (right) for MgO with and without the NAC correction.

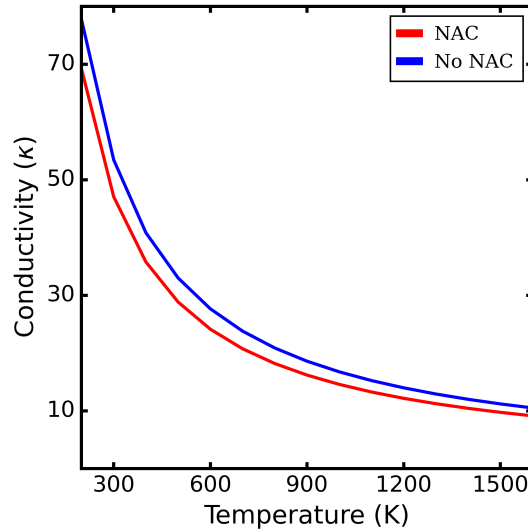


**Figure 11** Thermal conductivity versus temperature calculated from full inversion of the scattering matrix for MgO with and without the NAC correction.

QHKG methods, (iii) essential physical corrections (isotopic scattering, non-analytical terms), (iv) GPU acceleration and sparse tensor operations for large systems, and (v) modular Python design with extensive documentation and deployment tools.

Version 2.0 introduces significant advances over the original release [95], including native TDEP support for temperature-dependent force constants, seamless MLP integration via ASE and LAMMPS, flexible storage backends enabling 10,000+ atom simulations, anharmonicity diagnostics ( $\sigma_A$  score), and comprehensive testing/continuous integration. These enhancements position  $\kappa$ ALDO 2.0 as a premier tool for thermal transport research in complex materials.

Applications to  $\text{CsPbBr}_3$  and MgO demonstrate the software's capabilities for challenging systems:

perovskites requiring finite-temperature stabilization via TDEP and polar oxides needing non-analytical corrections. These examples illustrate workflows typical of contemporary materials science, combining multiple simulation packages and validation against experimental data.

Future development directions include: (i) hybrid MPI+GPU parallelization for multi-node scaling, (ii) automation of convergence testing for  $q$ -meshes and broadening parameters, (iii) four-phonon scattering for materials where three-phonon processes are insufficient (e.g., Si, diamond) [59], (iv) coupling to excited-state dynamics for electron-phonon and exciton-phonon interactions, and (v) integration with high-throughput frameworks (AiiDA, Atomate) for database generation.

We invite the community to contribute code, report issues, and propose new features via the GitHub repository. A discussions page (<https://github.com/nanotheorygroup/kaldo/discussions>) is available for questions, feature requests, and sharing workflows. With its open-source license, comprehensive documentation, and modular architecture,  $\kappa$ ALDo 2.0 aims to serve both as a production tool for applied research and a platform for method development in phonon transport theory.

## Data Availability

Input files, Jupyter notebooks, and results for all examples presented in this paper are available in the examples repository. A Docker image containing  $\kappa$ ALDo 2.0 and all dependencies can be obtained via `docker pull gbarbalinardo/kaldo:latest`.

## CPC Program Library Compliance

This manuscript adheres to the requirements specified in the Computer Physics Communications Program Library guidelines. The submitted package includes: (i) source code with test suite, (ii) installation instructions, (iii) example input/output files, (iv) auto-generated documentation, and (v) containerized environment for reproducibility.

## Acknowledgments

We are grateful to Riccardo Dettori, Frank Cerasoli, and Nicholas Martinez for helpful discussions and beta testing, and Mattias Perez and Higo de Araujo Oliveira for assistance in refining the example repository. This research was supported by the U.S. Department of Energy, Office of Basic Energy Sciences, Division of Materials Science and Engineering, grant DE-SC0022288. MIT Office of Research Computing and Data provided computing resources for performance benchmarks.

## References

- [1] Charles R Harris, K Jarrod Millman, Stéfan J Van Der Walt, Ralf Gommers, Pauli Virtanen, David Cournapeau, Eric Wieser, Julian Taylor, Sebastian Berg, Nathaniel J Smith, et al. Array programming with NumPy. *Nature*, 585(7825):357–362, 2020. doi: 10.1038/s41586-020-2649-2.
- [2] Pauli Virtanen, Ralf Gommers, Travis E Oliphant, Matt Haberland, Tyler Reddy, David Cournapeau, Evgeni Burovski, Pearu Peterson, Warren Weckesser, Jonathan Bright, et al. SciPy 1.0: fundamental algorithms for scientific computing in Python. *Nature Methods*, 17(3):261–272, 2020. doi: 10.1038/s41592-019-0686-2.
- [3] Martín Abadi, Ashish Agarwal, Paul Barham, Eugene Brevdo, Zhifeng Chen, Craig Citro, Greg S. Corrado, Andy Davis, Jeffrey Dean, Matthieu Devin, Sanjay Ghemawat, Ian Goodfellow, Andrew Harp, Geoffrey Irving, Michael Isard, Yangqing Jia, Rafal Jozefowicz, Lukasz Kaiser, Manjunath Kudlur, Josh Levenberg, Dan Mané, Rajat Monga, Sherry Moore, Derek Murray, Chris Olah, Mike Schuster, Jonathon Shlens, Benoit Steiner, Ilya Sutskever, Kunal Talwar, Paul Tucker, Vincent Vanhoucke, Vijay Vasudevan, Fernanda Viégas, Oriol Vinyals, Pete Warden, Martin Wattenberg, Martin Wicke, Yuan Yu, and Xiaoqiang Zheng. TensorFlow: Large-scale machine learning on heterogeneous systems, 2015. URL <https://www.tensorflow.org/>. Software available from tensorflow.org.
- [4] Ask Hjorth Larsen, Jens Jørgen Mortensen, Jakob Blomqvist, Ivano E. Castelli, Rune Christensen, Marcin Dułak, Jesper Friis, Michael N. Groves, Bjørk Hammer, Cory Hargus, Eric D. Hermes, Paul C. Jennings, Peter Bjerre Jensen, James Kermode, John R. Kitchin, Esben Leonhard Kolsbjerg, Joseph Kubal, Kristen Kaasbjerg, Steen Lysgaard, Jón Bergmann Maronsson, Tristan Maxson, Thomas Olsen, Lars Pastewka, Andrew Peterson, Carsten Rostgaard, Jakob Schiøtz, Ole Schütt, Mikkel Strange, Kristian S. Thygesen, Tejs Vegge, Lasse Vilhelmsen, Michael Walter, Zhenhua Zeng, and Karsten W. Jacobsen. The atomic simulation environment—a Python library for working with atoms. *Journal of Physics: Condensed Matter*, 29(27):273002, June 2017. doi: 10.1088/1361-648X/aa680e. URL <https://dx.doi.org/10.1088/1361-648X/aa680e>.
- [5] Daniel GA Smith and Johnnie Gray. opt\_einsum – a Python package for optimizing contraction order for einsum-like expressions. *Journal of Open Source Software*, 3(26):753, 2018. doi: 10.21105/joss.00753.
- [6] Andrew Collette. Python and HDF5: Unlocking scientific data. 2014.
- [7] Yoyo Hinuma, Giovanni Pizzi, Yu Kumagai, Fumiyasu Oba, and Isao Tanaka. Band structure diagram paths based on crystallography. *Computational Materials Science*, 128:140–184, 2017. doi: 10.1016/j.commatsci.2016.10.015.
- [8] David G Cahill, Wayne K Ford, Kenneth E Goodson, Gerald D Mahan, Arunava Majumdar, Humphrey J Maris, Roberto Merlin, and Simon R Phillpot. Nanoscale thermal transport. *Journal of Applied Physics*, 93(2):793–818, 2003.
- [9] David G. Cahill, Paul V. Braun, Gang Chen, David R. Clarke, Shanhui Fan, Kenneth E. Goodson, Pawel Keblinski, William P. King, Gerald D. Mahan, Arun Majumdar, Humphrey J. Maris, Simon R. Phillpot, Eric Pop, and Li Shi. Nanoscale thermal transport. II. 2003–2012. *Applied*

- Physics Reviews*, 1(1):011305, March 2014. doi: 10.1063/1.4832615. URL <http://aip.scitation.org/doi/10.1063/1.4832615>.
- [10] Li Shi, Chris Dames, Jennifer R. Lukes, Pramod Reddy, John Duda, David G. Cahill, Jaeho Lee, Amy Marconnet, Kenneth E. Goodson, Je-Hyeong Bahk, Ali Shakouri, Ravi S. Prasher, Jonathan Felts, William P. King, Bumsoo Han, and John C. Bischof. Evaluating Broader Impacts of Nanoscale Thermal Transport Research. *Nanoscale and Microscale Thermophysical Engineering*, 19(2):127–165, April 2015. doi: 10.1080/15567265.2015.1031857. URL <http://www.tandfonline.com/doi/full/10.1080/15567265.2015.1031857>.
- [11] Stefano Curtarolo, Wahyu Setyawan, Gus LW Hart, Michal Jahnatek, Roman V Chepulskii, Richard H Taylor, Shidong Wang, Junkai Xue, Kesong Yang, Ohad Levy, et al. Aflow: An automatic framework for high-throughput materials discovery. *Computational Materials Science*, 58:218–226, 2012.
- [12] Anubhav Jain, Shyue Ping Ong, Geoffroy Hautier, Wei Chen, William Davidson Richards, Stephen Dacek, Shreyas Cholia, Dan Gunter, David Skinner, Gerbrand Ceder, and Kristin A. Persson. Commentary: The Materials Project: A materials genome approach to accelerating materials innovation. *APL Materials*, 1(1):011002, July 2013. doi: 10.1063/1.4812323. URL <https://doi.org/10.1063/1.4812323>.
- [13] Scott Kirklin, James E Saal, Bryce Meredig, Alex Thompson, Jeff W Doak, Muratahan Aykol, Stephan Rühl, and Chris Wolverton. The open quantum materials database (oqmd): assessing the accuracy of dft formation energies. *npj Computational Materials*, 1(1):15010, 2015.
- [14] Ivan Carnimeo, Fabio Affinito, Stefano Baroni, Oscar Baseggio, Laura Bellentani, Riccardo Bertossa, Pietro Davide Delugas, Fabrizio Ferrari Ruffino, Sergio Orlandini, Filippo Spiga, et al. Quantum espresso: One further step toward the exascale. *Journal of Chemical Theory and Computation*, 19(20):6992–7006, 2023. URL <https://doi.org/10.1021/acs.jctc.3c00249>.
- [15] Jörg Behler and Michele Parrinello. Generalized Neural-Network Representation of High-Dimensional Potential-Energy Surfaces. *Phys. Rev. Lett.*, 98(14):146401, 2007. doi: 10.1103/PhysRevLett.98.146401. URL <https://link.aps.org/doi/10.1103/PhysRevLett.98.146401>.
- [16] Albert P. Bartók, Mike C. Payne, Risi Kondor, and Gábor Csányi. Gaussian Approximation Potentials: The Accuracy of Quantum Mechanics, without the Electrons. *Phys. Rev. Lett.*, 104(13):136403, 2010. doi: 10.1103/PhysRevLett.104.136403. URL <https://link.aps.org/doi/10.1103/PhysRevLett.104.136403>.
- [17] Alexander V. Shapeev. Moment Tensor Potentials: A Class of Systematically Improvable Interatomic Potentials. *Multiscale Model. Simul.*, 14(3):1153–1173, January 2016. doi: 10.1137/15M1054183. URL <https://epubs.siam.org/doi/10.1137/15M1054183>.
- [18] A.P. Thompson, L.P. Swiler, C.R. Trott, S.M. Foiles, and G.J. Tucker. Spectral neighbor analysis method for automated generation of quantum-accurate interatomic potentials. *Journal of Computational Physics*, 285:316–330, March 2015. doi: 10.1016/j.jcp.2014.12.018. URL <https://linkinghub.elsevier.com/retrieve/pii/S0021999114008353>.
- [19] Linfeng Zhang, Jiequn Han, Han Wang, Roberto Car, and Weinan E. Deep Potential Molecular Dynamics: A Scalable Model with the Accuracy of Quantum Mechanics. *Phys. Rev. Lett.*, 120

- (14):143001, 2018. doi: 10.1103/PhysRevLett.120.143001. URL <https://link.aps.org/doi/10.1103/PhysRevLett.120.143001>.
- [20] Ralf Drautz. Atomic cluster expansion for accurate and transferable interatomic potentials. *Phys. Rev. B*, 99(1):014104, 2019. doi: 10.1103/PhysRevB.99.014104. URL <https://link.aps.org/doi/10.1103/PhysRevB.99.014104>.
- [21] Zheyong Fan, Zezhu Zeng, Cunzhi Zhang, Yanzhou Wang, Keke Song, Haikuan Dong, Yue Chen, and Tapio Ala-Nissila. Neuroevolution machine learning potentials: Combining high accuracy and low cost in atomistic simulations and application to heat transport. *Physical Review B*, 104(10):104309, September 2021. doi: 10.1103/PhysRevB.104.104309. URL <https://link.aps.org/doi/10.1103/PhysRevB.104.104309>.
- [22] Simon Batzner, Albert Musaelian, Lixin Sun, Mario Geiger, Jonathan P. Mailoa, Mordechai Kornbluth, Nicola Molinari, Tess E. Smidt, and Boris Kozinsky. E(3)-equivariant graph neural networks for data-efficient and accurate interatomic potentials. *Nature Commun.*, 13(1):2453, May 2022. doi: 10.1038/s41467-022-29939-5. URL <https://www.nature.com/articles/s41467-022-29939-5>.
- [23] Chi Chen and Shyue Ping Ong. A universal graph deep learning interatomic potential for the periodic table. *Nat Comput Sci*, 2(11):718–728, November 2022. doi: 10.1038/s43588-022-00349-3. URL <https://www.nature.com/articles/s43588-022-00349-3>.
- [24] Han Yang, Chenxi Hu, Yichi Zhou, Xixian Liu, Yu Shi, Jielan Li, Guanzhi Li, Zekun Chen, Shuizhou Chen, Claudio Zeni, Matthew Horton, Robert Pinsler, Andrew Fowler, Daniel Zügner, Tian Xie, Jake Smith, Lixin Sun, Qian Wang, Lingyu Kong, Chang Liu, Hongxia Hao, and Ziheng Lu. MatterSim: A deep learning atomistic model across elements, temperatures and pressures, 2024.
- [25] Mark Duschatko, Sajant Dasgupta, Jonathan Abed, Marwène Bouaziz, Janosh Barroso, Kristin A. Persson, and Anubhav Jain. Orb: A Fast, Accurate, Openly-licensed Materials Model trained on 118 elements, 2024. URL <http://arxiv.org/abs/2410.22570>. arXiv:2410.22570 [cond-mat, physics:physics].
- [26] Ilyes Batatia, Philipp Benner, Yuan Chiang, Alin M Elena, Dávid P Kovács, Janosh Riebesell, Xavier R Advincula, Mark Asta, Matthew Avaylon, William J Baldwin, et al. A foundation model for atomistic materials chemistry. *The Journal of Chemical Physics*, 163(18), 2025.
- [27] Melville S. Green. Markoff Random Processes and the Statistical Mechanics of Time-Dependent Phenomena. II. Irreversible Processes in Fluids. *J. Chem. Phys.*, 22(3):398–413, 1954. doi: 10.1063/1.1740082. URL <https://doi.org/10.1063/1.1740082>.
- [28] Ryogo Kubo. Statistical-Mechanical Theory of Irreversible Processes. I. General Theory and Simple Applications to Magnetic and Conduction Problems. *J. Phys. Soc. Jpn.*, 12(6):570–586, June 1957. doi: 10.1143/JPSJ.12.570. URL <https://journals.jps.jp/doi/10.1143/JPSJ.12.570>.
- [29] R. Zwanzig. Time-Correlation Functions and Transport Coefficients in Statistical Mechanics. *Annual Review of Physical Chemistry*, 16(Volume 16.):67–102, 1965. doi: 10.1146/annurev.pc.16.100165.000435. URL <https://www.annualreviews.org/content/journals/10.1146/annurev.pc.16.100165.000435>.

- [30] Anthony J. C. Ladd, Bill Moran, and William G. Hoover. Lattice thermal conductivity: A comparison of molecular dynamics and anharmonic lattice dynamics. *Phys. Rev. B*, 34(8): 5058–5064, 1986. doi: 10.1103/PhysRevB.34.5058. URL <https://link.aps.org/doi/10.1103/PhysRevB.34.5058>.
- [31] Florian Müller-Plathe. A simple nonequilibrium molecular dynamics method for calculating the thermal conductivity. *The Journal of Chemical Physics*, 106(14):6082–6085, 1997. doi: 10.1063/1.473271.
- [32] Patrick K. Schelling, Simon R. Phillpot, and Pawel Keblinski. Comparison of atomic-level simulation methods for computing thermal conductivity. *Physical Review B*, 65(14):144306, 2002. doi: 10.1103/PhysRevB.65.144306.
- [33] Gabriele C. Sosso, Davide Donadio, Sebastiano Caravati, Jörg Behler, and Marco Bernasconi. Thermal transport in phase-change materials from atomistic simulations. *Phys. Rev. B*, 86(10):104301, 2012. doi: 10.1103/PhysRevB.86.104301. URL <https://link.aps.org/doi/10.1103/PhysRevB.86.104301>.
- [34] Claudia Mangold, Shunda Chen, Giuseppe Barbalinardo, Jörg Behler, Pascal Pochet, Konstantinos Termentzidis, Yang Han, Laurent Chaput, David Lacroix, and Davide Donadio. Transferability of neural network potentials for varying stoichiometry: Phonons and thermal conductivity of  $\text{Mn}_x\text{Ge}_y$  compounds. *Journal of Applied Physics*, 127(24):244901, 2020. doi: 10.1063/5.0009550. URL <http://aip.scitation.org/doi/10.1063/5.0009550>.
- [35] Marcel F. Langer, Florian Knoop, Christian Carbogno, Matthias Scheffler, and Matthias Rupp. Heat flux for semilocal machine-learning potentials. *Phys. Rev. B*, 108(10):L100302, 2023. doi: 10.1103/PhysRevB.108.L100302. URL <https://link.aps.org/doi/10.1103/PhysRevB.108.L100302>.
- [36] Haikuan Dong, Yongbo Shi, Penghua Ying, Ke Xu, Ting Liang, Yanzhou Wang, Zezhu Zeng, Xin Wu, Wenjiang Zhou, Shiyun Xiong, Shunda Chen, and Zheyong Fan. Molecular dynamics simulations of heat transport using machine-learned potentials: A mini-review and tutorial on GPUMD with neuroevolution potentials. *Journal of Applied Physics*, 135(16):161101, 2024. doi: 10.1063/5.0200833. URL <https://doi.org/10.1063/5.0200833>.
- [37] Aris Marcolongo, Paolo Umari, and Stefano Baroni. Microscopic theory and quantum simulation of atomic heat transport. *Nature Phys*, 12(1):80–84, 2016. doi: 10.1038/nphys3509. URL <http://www.nature.com/articles/nphys3509>.
- [38] John M. Ziman. *Electrons and Phonons: The Theory of Transport Phenomena in Solids*. Oxford Classic Texts in the Physical Sciences. Oxford University Press, Oxford, 2001. ISBN 978-0-19-850779-6.
- [39] Gyaneshwar P Srivastava. *The physics of phonons*. CRC press, 2022.
- [40] Michele Simoncelli, Nicola Marzari, and Francesco Mauri. Unified theory of thermal transport in crystals and glasses. *Nature Physics*, 15(8):809–813, August 2019. doi: 10.1038/s41567-019-0520-x. URL <https://www.nature.com/articles/s41567-019-0520-x>.

- [41] Leyla Isaeva, Giuseppe Barbalinardo, Davide Donadio, and Stefano Baroni. Modeling heat transport in crystals and glasses from a unified lattice-dynamical approach. *Nature Communications*, 10(1):3853, August 2019. doi: 10.1038/s41467-019-11572-4. URL <https://www.nature.com/articles/s41467-019-11572-4>.
- [42] Sanghamitra Neogi and Davide Donadio. Anisotropic In-Plane Phonon Transport in Silicon Membranes Guided by Nanoscale Surface Resonators. *Phys. Rev. Applied*, 14(2):024004, August 2020. doi: 10.1103/PhysRevApplied.14.024004. URL <https://link.aps.org/doi/10.1103/PhysRevApplied.14.024004>.
- [43] N Lundgren, P Erhart, and D Donadio. Mode-projected heat capacity and the anomalous thermal conductivity of ferroelectric relaxor perovskites. *Physical Review B*, 103(22):224207, 2021.
- [44] Michele Simoncelli, Nicola Marzari, and Francesco Mauri. Wigner formulation of thermal transport in solids. *Physical Review X*, 12(4):041011, 2022.
- [45] Zhongwei Zhang, Yangyu Guo, Marc Bescond, Jie Chen, Masahiro Nomura, and Sebastian Volz. How coherence is governing diffuson heat transfer in amorphous solids. *npj Computational Materials*, 8(1):96, 2022.
- [46] Alfredo Fiorentino, Paolo Pegolo, Stefano Baroni, and Davide Donadio. Effects of colored disorder on the heat conductivity of sige alloys from first principles. *Physical Review B*, 111(13):134205, 2025.
- [47] Michele Simoncelli, Francesco Mauri, and Nicola Marzari. Thermal conductivity of glasses: first-principles theory and applications. *npj Computational Materials*, 9:106, 2023. doi: 10.1038/s41524-023-01033-4.
- [48] Olle Hellman and I. A. Abrikosov. Temperature-dependent effective third-order interatomic force constants from first principles. *Physical Review B*, 88(14):144301, October 2013. doi: 10.1103/PhysRevB.88.144301. URL <https://link.aps.org/doi/10.1103/PhysRevB.88.144301>.
- [49] Aloïs Castellano, JP Batista, and Matthieu J Verstraete. Mode-coupling theory of lattice dynamics for classical and quantum crystals. *J. Chem. Phys.*, 159(23), 2023.
- [50] Florian Knoop, Nina Shulumba, Aloïs Castellano, J. P. Alvarinhas Batista, Roberta Farris, Matthieu J. Verstraete, Matthew Heine, David Broido, Dennis S. Kim, Johan Klarbring, Igor A. Abrikosov, Sergei I. Simak, and Olle Hellman. TDEP: Temperature dependent effective potentials. *Journal of Open Source Software*, 9(94):6264, 2024. doi: 10.21105/joss.06264.
- [51] Dylan A Folkner, Zekun Chen, Giuseppe Barbalinardo, Florian Knoop, and Davide Donadio. Elastic moduli and thermal conductivity of quantum materials at finite temperature. *Journal of Applied Physics*, 136(22), 2024.
- [52] Wu Li, Jesús Carrete, Nebil A Katcho, and Natalio Mingo. Shengbte: A solver of the boltzmann transport equation for phonons. *Computer Physics Communications*, 185(6):1747–1758, 2014.
- [53] Atsushi Togo, Laurent Chaput, Terumasa Tadano, and Isao Tanaka. First-principles phonon calculations with phonopy and phono3py. *Journal of the Physical Society of Japan*, 92(1):012001, 2023.

- [54] Andrea Cepellotti, Jennifer Coulter, Anders Johansson, Natalya S Fedorova, and Boris Kozinsky. Phoebe: a high-performance framework for solving phonon and electron Boltzmann transport equations. *J. Phys. Mater.*, 5(3):035003, August 2022. doi: 10.1088/2515-7639/ac86f6. URL <https://doi.org/10.1088/2515-7639/ac86f6>.
- [55] T. Tadano, Y. Gohda, and S. Tsuneyuki. Anharmonic force constants extracted from first-principles molecular dynamics: applications to heat transfer simulations. *J. Phys.: Condens. Matter*, 26(22):225402, May 2014. doi: 10.1088/0953-8984/26/22/225402. URL <https://dx.doi.org/10.1088/0953-8984/26/22/225402>.
- [56] Safoura Nayeb Sadeghi, Sangyeop Lee, and Keivan Esfarjani. THERMACOND, a code to compute lattice thermal conductivity from harmonic and anharmonic force constants. *npj Comput Mater*, 11(1):303, 2025. doi: 10.1038/s41524-025-01673-8. URL <https://www.nature.com/articles/s41524-025-01673-8>.
- [57] Lorenzo Paulatto, Francesco Mauri, and Michele Lazzeri. Anharmonic properties from a generalized third-order ab initio approach: Theory and applications to graphite and graphene. *Physical Review B*, 87(21):214303, June 2013. doi: 10.1103/PhysRevB.87.214303. URL <https://link.aps.org/doi/10.1103/PhysRevB.87.214303>.
- [58] Giorgia Fugallo, Michele Lazzeri, Lorenzo Paulatto, and Francesco Mauri. Ab initio variational approach for evaluating lattice thermal conductivity. *Phys. Rev. B*, 88(4):045430, July 2013. doi: 10.1103/PhysRevB.88.045430. URL <https://link.aps.org/doi/10.1103/PhysRevB.88.045430>.
- [59] Tianli Feng and Xiulin Ruan. Four-phonon scattering significantly reduces intrinsic thermal conductivity of solids. *Physical Review B*, 96(16):161201, 2017.
- [60] Tianli Feng and Xiulin Ruan. Four-phonon scattering reduces intrinsic thermal conductivity of graphene and the contributions from flexural phonons. *Phys. Rev. B*, 97(4):045202, 2018. doi: 10.1103/PhysRevB.97.045202. URL <https://link.aps.org/doi/10.1103/PhysRevB.97.045202>.
- [61] Aidan P Thompson, H Metin Aktulga, Richard Berger, Dan S Bolintineanu, W Michael Brown, Paul S Crozier, Pieter J In't Veld, Axel Kohlmeyer, Stan G Moore, Trung Dac Nguyen, et al. LAMMPS—a flexible simulation tool for particle-based materials modeling at the atomic, meso, and continuum scales. *Computer Physics Communications*, 271:108171, 2022.
- [62] Zheyong Fan, Yanzhou Wang, Penghua Ying, Keke Song, Junjie Wang, Yong Wang, Zezhu Zeng, Ke Xu, Eric Lindgren, J. Magnus Rahm, Alexander J. Gabourie, Jiahui Liu, Haikuan Dong, Jianyang Wu, Yue Chen, Zheng Zhong, Jian Sun, Paul Erhart, Yanjing Su, and Tapio Ala-Nissila. GPUMD: A package for constructing accurate machine-learned potentials and performing highly efficient atomistic simulations. *The Journal of Chemical Physics*, 157(11):114801, September 2022. doi: 10.1063/5.0106617. URL <https://doi.org/10.1063/5.0106617>.
- [63] Han Wang, Linfeng Zhang, Jiequn Han, and E Weinan. Deepmd-kit: A deep learning package for many-body potential energy representation and molecular dynamics. *Computer Physics Communications*, 228:178–184, 2018.

- [64] Rudolf Peierls. Zur kinetischen Theorie der Wärmeleitung in Kristallen. *Annalen der Physik*, 3(8):1055–1101, 1929. doi: 10.1002/andp.19293950803.
- [65] A Ward, DA Broido, DA Stewart, and G Deinzer. Ab initio theory of the lattice thermal conductivity in diamond. *Physical Review B*, 80(12):125203, 2009.
- [66] M. Omini and A. Sparavigna. Beyond the isotropic-model approximation in the theory of thermal conductivity. *Phys. Rev. B*, 53(14):9064–9073, 1996. doi: 10.1103/PhysRevB.53.9064. URL <https://link.aps.org/doi/10.1103/PhysRevB.53.9064>.
- [67] D. A. Broido, A. Ward, and N. Mingo. Lattice thermal conductivity of silicon from empirical interatomic potentials. *Phys. Rev. B*, 72(1):014308, 2005. doi: 10.1103/PhysRevB.72.014308. URL <https://link.aps.org/doi/10.1103/PhysRevB.72.014308>.
- [68] Andrea Cepellotti and Nicola Marzari. Thermal Transport in Crystals as a Kinetic Theory of Relaxons. *Physical Review X*, 6(4):041013, October 2016. doi: 10.1103/PhysRevX.6.041013. URL <https://link.aps.org/doi/10.1103/PhysRevX.6.041013>.
- [69] Subhash L. Shindé and Gyaneshwar P. Srivastava, editors. *Length-Scale Dependent Phonon Interactions*, volume 128 of *Topics in Applied Physics*. Springer New York, New York, NY, 2014. ISBN 978-1-4614-8650-3 978-1-4614-8651-0. doi: 10.1007/978-1-4614-8651-0. URL <http://link.springer.com/10.1007/978-1-4614-8651-0>.
- [70] Giuliano Benenti, Davide Donadio, Stefano Lepri, and Roberto Livi. Non-Fourier heat transport in nanosystems. *La Rivista del Nuovo Cimento*, 46(3):105–161, March 2023. doi: 10.1007/s40766-023-00041-w. URL <https://doi.org/10.1007/s40766-023-00041-w>.
- [71] Keith T. Regner, Daniel P. Sellan, Zonghui Su, Cristina H. Amon, Alan J.H. McGaughey, and Jonathan A. Malen. Broadband phonon mean free path contributions to thermal conductivity measured using frequency domain thermoreflectance. *Nat Commun*, 4(1):1640, 2013. URL <http://www.nature.com/articles/ncomms2630>.
- [72] Jesse Maassen and Mark Lundstrom. A simple Boltzmann transport equation for ballistic to diffusive transient heat transport. *Journal of Applied Physics*, 117(13):135102, 2015. doi: 10.1063/1.4916245. URL <https://aip.scitation.org/doi/full/10.1063/1.4916245>.
- [73] J. Kaiser, T. Feng, J. Maassen, X. Wang, X. Ruan, and M. Lundstrom. Thermal transport at the nanoscale: A Fourier’s law vs. phonon Boltzmann equation study. *J. Appl. Phys.*, 121(4):044302, 2017. doi: 10.1063/1.4974872. URL <https://aip.scitation.org/doi/full/10.1063/1.4974872>.
- [74] Andrea Cepellotti and Nicola Marzari. Boltzmann Transport in Nanostructures as a Friction Effect. *Nano Lett.*, 17(8):4675–4682, August 2017. doi: 10.1021/acs.nanolett.7b01202. URL <https://pubs.acs.org/doi/10.1021/acs.nanolett.7b01202>.
- [75] Philip B Allen and Joseph L Feldman. Thermal conductivity of glasses: Theory and application to amorphous si. *Physical review letters*, 62(6):645, 1989.
- [76] Philip B Allen and Joseph L Feldman. Thermal conductivity of disordered harmonic solids. *Physical Review B*, 48(17):12581, 1993.

- [77] Alfredo Fiorentino and Stefano Baroni. From Green-Kubo to the full Boltzmann kinetic approach to heat transport in crystals and glasses. *Physical Review B*, 107(5):054311, February 2023. doi: 10.1103/PhysRevB.107.054311. URL <https://link.aps.org/doi/10.1103/PhysRevB.107.054311>.
- [78] Philip B Allen, Joseph L Feldman, Jaroslav Fabian, and Frederick Wooten. Diffusons, locons and propagons: Character of atomic vibrations in amorphous si. *Philosophical Magazine B*, 79(11-12):1715–1731, 1999.
- [79] Đorđe Dangić, Olle Hellman, Stephen Fahy, and Ivana Savić. The origin of the lattice thermal conductivity enhancement at the ferroelectric phase transition in GeTe. *npj Comput Mater*, 7:57, December 2021. doi: 10.1038/s41524-021-00523-7. URL <http://www.nature.com/articles/s41524-021-00523-7>.
- [80] Shin-ichiro Tamura. Isotope scattering of dispersive phonons in Ge. *Physical Review B*, 27(2):858–866, January 1983. doi: 10.1103/PhysRevB.27.858. URL <https://link.aps.org/doi/10.1103/PhysRevB.27.858>.
- [81] Jivtesh Garg, Nicola Bonini, Boris Kozinsky, and Nicola Marzari. Role of disorder and anharmonicity in the thermal conductivity of silicon-germanium alloys: A first-principles study. *Physical review letters*, 106(4):045901, 2011.
- [82] Xavier Gonze and Changyol Lee. Dynamical matrices, born effective charges, dielectric permittivity tensors, and interatomic force constants from density-functional perturbation theory. *Physical Review B*, 55(16):10355, 1997.
- [83] Giuseppe Barbalinardo, Zekun Chen, Haikuan Dong, Zheyong Fan, and Davide Donadio. Ultra-high Convergent Thermal Conductivity of Carbon Nanotubes from Comprehensive Atomistic Modeling. *Phys. Rev. Lett.*, 127(2):025902, 2021. doi: 10.1103/PhysRevLett.127.025902. URL <https://link.aps.org/doi/10.1103/PhysRevLett.127.025902>.
- [84] Nicolas Mounet and Nicola Marzari. First-principles determination of the structural, vibrational and thermodynamic properties of diamond, graphite, and derivatives. *Physical Review B*, 71(20):205214, 2005.
- [85] Slawomir Biernacki and Matthias Scheffler. Negative thermal expansion of diamond and zincblende semiconductors. *Phys. Rev. Lett.*, 63(3):290–293, July 1989. doi: 10.1103/PhysRevLett.63.290. URL <https://link.aps.org/doi/10.1103/PhysRevLett.63.290>.
- [86] A. Fleszar and X. Gonze. First-principles thermodynamical properties of semiconductors. *Phys. Rev. Lett.*, 64(24):2961–2961, June 1990. doi: 10.1103/PhysRevLett.64.2961. URL <https://link.aps.org/doi/10.1103/PhysRevLett.64.2961>.
- [87] Stefano Baroni, Paolo Giannozzi, and Eyvaz Isaev. Thermal properties of materials from ab-initio quasi-harmonic phonons. *Reviews in Mineralogy and Geochemistry*, 71:39–57, 2010. doi: 10.2138/rmg.2010.71.3. URL <http://arxiv.org/abs/1112.4977>.
- [88] Florian Knoop, Thomas AR Purcell, Matthias Scheffler, and Christian Carbogno. Anharmonicity measure for materials. *Physical Review Materials*, 4(8):083809, 2020.

- [89] Jerry Tersoff. New empirical approach for the structure and energy of covalent systems. *Physical review B*, 37(12):6991, 1988.
- [90] Filippo Bigi, Paolo Pegolo, Arslan Mazitov, and Michele Ceriotti. Pushing the limits of unconstrained machine-learned interatomic potentials. *arXiv preprint arXiv:2601.16195*, 2026.
- [91] Erik Fransson, Julia Wiktor, and Paul Erhart. Phase transitions in inorganic halide perovskites from machine-learned potentials. *The Journal of Physical Chemistry C*, 127(28):13773–13781, 2023. doi: 10.1021/acs.jpcc.3c01542. URL <https://doi.org/10.1021/acs.jpcc.3c01542>.
- [92] Đorđe Dangić, Giovanni Caldarelli, Raffaello Bianco, Ivana Savić, and Ion Errea. Lattice thermal conductivity in the anharmonic overdamped regime. *Phys. Rev. B*, 111(10):104314, March 2025. doi: 10.1103/PhysRevB.111.104314. URL <https://link.aps.org/doi/10.1103/PhysRevB.111.104314>.
- [93] P. Giannozzi, O. Andreussi, T. Brumme, O. Bunau, M. Buongiorno Nardelli, M. Calandra, R. Car, C. Cavazzoni, D. Ceresoli, M. Cococcioni, N. Colonna, I. Carnimeo, A. Dal Corso, S. de Gironcoli, P. Delugas, R. A. DiStasio, A. Ferretti, A. Floris, G. Fratesi, G. Fugallo, R. Gebauer, U. Gerstmann, F. Giustino, T. Gorni, J. Jia, M. Kawamura, H.-Y. Ko, A. Kokalj, E. Küçükbenli, M. Lazzeri, M. Marsili, N. Marzari, F. Mauri, N. L. Nguyen, H.-V. Nguyen, A. Otero-de-la Roza, L. Paulatto, S. Poncé, D. Rocca, R. Sabatini, B. Santra, M. Schlipf, A. P. Seitsonen, A. Smogunov, I. Timrov, T. Thonhauser, P. Umari, N. Vast, X. Wu, and S. Baroni. Advanced capabilities for materials modelling with Quantum ESPRESSO. *Journal of Physics: Condensed Matter*, 29(46):465901, October 2017. doi: 10.1088/1361-648X/aa8f79. URL <https://dx.doi.org/10.1088/1361-648X/aa8f79>.
- [94] D. R. Hamann. Optimized norm-conserving Vanderbilt pseudopotentials. *Physical Review B*, 88(8):085117, August 2013. doi: 10.1103/PhysRevB.88.085117. URL <https://link.aps.org/doi/10.1103/PhysRevB.88.085117>.
- [95] Giuseppe Barbalinardo, Zekun Chen, Nicholas W Lundgren, and Davide Donadio. Efficient anharmonic lattice dynamics calculations of thermal transport in crystalline and disordered solids. *Journal of Applied Physics*, 128(13):135104, 2020.